HOKKAIDO UNIVERSITY

Title	Shape-Controlled Growth of MgH2/Mg Nano/Microstructures Via Hydriding Chemical Vapor Deposition
Author(s)	Zhu, Chunyu; Hosokai, Sou; Matsumoto, Itoko et al.
Citation	Crystal Growth & Design, 10(12), 5123-5128 https://doi.org/10.1021/cg100856n
Issue Date	2010
Doc URL	https://hdl.handle.net/2115/48525
Type	journal article
File Information	CGD10_5123-5128.pdf

Hokkaido University Collection of Scholarly and Academic Papers : HUSCAP

Shape-Controlled Growth of MgH_2/Mg Nano/Microstructures Via Hydriding Chemical Vapor Deposition

Chunyu Zhu [†] *Sou Hosokai,* [†] *Itoko Matsumoto,* [‡] *Tomohiro Akiyama,* [* †]

† Center for Advanced Research of Energy Conversion Materials, Hokkaido University, Sapporo 060-8628, Japan

‡ Energy Technology Research Institute, National Institute of Advanced Industrial Science and Technology, Ibaraki 305-8565, Japan

* Corresponding author, Tel.: +81-11-706-6842; Fax: +81-11-726-0731.

Email: takiyama@eng.hokudai.ac.jp

ABSTRACT

In this paper, we report the shape-controlled growth of MgH_2/Mg nano/microstructures via hydriding chemical vapor deposition (HCVD), wherein magnesium vapor was deposited on a substrate at different temperatures ranging from 225 °C to 600 °C and H_2 pressures ranging from 1 to 4 MPa. The products obtained after heating for 7, 13, and 20 h were identified by XRD and observed by SEM. The shape, size, and purity of the products strongly depended on the experimental conditions, which were classified according to the P-T equilibrium diagram for MgH_2. The diagram showed six distinct areas for the products MgH_2 and/or Mg having the following structures: fine and coarse powder, dendrite, root-like structure, straight and curved fibers, irregular bulk structure, and hexagonal and spherical structures. The diagram can be used quite effectively for controlling the shape of MgH_2 and/or Mg, and this may lay the foundation for the mass production of nano/microsized MgH_2/Mg for use in hydrogen storage or batteries.

KEYWORDS Hydrogen storage, magnesium hydride, nanostuctures, crystal growth, hydriding chemical vapor deposition

Introduction

Crystal growth of nano/micro materials has received increased attention because these materials exhibit unique properties and can be used in various applications.[1,2] In this respect, the synthesis of Mg/MgH_2 nano/microstructures could be of interest in the field of hydrogen storage and batteries.[3-7] Magnesium hydride (MgH_2), which contains 7.6 mass% of hydrogen, is a promising candidate for hydrogen storage applications because of the relative abundance of Mg resources, low weight of Mg, and the high hydrogen content of MgH_2.[8] However, its applications have been limited by its high operation temperature of 300 °C at an equilibrium pressure of 0.1 MPa and the slow hydrogen adsorption kinetics of bulk Mg.[9] To overcome these drawbacks, most studies have focused on the preparation of Mg/MgH_2 nano/microstructures and nanocomposites.[3,4,10-20] Mechanical milling of Mg/MgH_2 with appropriate elements, alloys, or compounds is the most widely used method for producing such Mg-based nanomaterials.[3,16,17] These materials have greatly contributed to elucidating the relationship between reactivity and nanostructure. Although some doping or alloying techniques can affect the desorption temperature, this always lowers the hydrogen storage capacity because of the additional weight. With the milling technique, the particle size of MgH_2 can be reduced to several hundreds of nanometers while the grain size can be reduced to several tens of nanometers; however, in most cases, this is always accompanied by inhomogeneous size distributions, agglomeration, and impurities. Recently, Mg nanowires with diameters ranging from 30 to 170 nm were produced via a physical vapor-transport deposition method; these nanowires showed enhanced kinetics for hydrogen adsorption.[4] Most significantly, the desorption energy of MgH_2 (energy needed for the dissociation of MgH_2 to Mg and H_2; it is 74 kJ/mol-H_2 for the bulk form), drastically decreased to 65.3 kJ/mol-H_2 for nanowires with diameters of 30–50 nm. Hydriding chemical vapor depostion (HCVD)[18] is another method used to produce MgH_2 fibers (or wires in the nano/microscale) with high purity. These fibers were synthesized by depositing the vaporized Mg under H_2 atmosphere, as expressed by the gas-gas reaction:

$$H_2\,(g) + Mg\,(g) \rightarrow MgH_2\,(s) \qquad (1)$$

The as-prepared MgH_2 fibers showed excellent H_2 storage properties.[19] MgH_2/Mg nano/microstructures are expected to depend on temperature and hydrogen pressure.[20,21] Historically, Dr. Ukichiro Nakaya of Hokkaido University, Sapporo, is world-famous for elucidating the relationship between the shape of snow crystals and the atmospheric conditions, i.e., temperature and supersaturation of the atmosphere.[22] Weather conditions are now easily predicted thanks to the Nakaya diagram. In this respect, the synthesis of MgH_2/Mg nano/microstructures with shapes controlled under different temperature and hydrogen pressure may be of considerable interest for researchers in the field of hydrogen storage or batteries.[21] The P-T diagram for MgH_2/Mg would be of great help in material design or mass production.

In this study, we carried out the controlled synthesis of MgH_2/Mg nano/microstructures. We succeeded in controlling the shapes (nanofibers, nanoparticles, microdendrites, irregular bulk, hexagonal microplates, and microspheres) and compositions of the products by adjusting the deposition temperature and H_2 pressure. The results were plotted on a thermodynamic P-T (pressure-temperature) diagram on basis of the dissociation of MgH_2, as shown in Figure S1:

$$MgH_2\,(s) \leftrightarrow H_2\,(g) + Mg\,(s) \qquad (2)$$

Thermodynamically, the white area denotes the stable phase of MgH_2; the shadowed area indicates MgH_2 dissociating into Mg and H_2 under high temperatures. Theoretically, we should be able to produce MgH_2 in the MgH_2 stable area and Mg in the decomposition area. More details are presented in the following sections.

Experimental section

MgH_2/Mg products were prepared from commercially available Mg (purity 99.9%, particle size < 75 μm) under a highly pure H_2 atmosphere (99.99999%). The experimental setup was modified from ref. [21] as shown in Figure S2-(a): a cooler jacket running with cooled water was set around the left-hand flange of the Inconel tube reactor to produce a larger temperature distribution along the tube wall. A piece of stainless mesh (100 mesh, Φ0.10 × 100 × 220 mm, SUS304, Nilaco Ltd.) adhered along the tube wall was used as the substrate for collecting the products. Five grams of raw Mg were heated to vaporization at 600 ºC under 1, 2, 3, and 4 MPa of H_2; the reactants of H_2 and Mg vapor were deposited onto the cooled substrate and formed MgH_2/Mg products. Heating times of 7, 13, and 20 h were used; after several hours of heating, the reactor was cooled down to room temperature in about 1 hour by a fan, during which time the H_2 pressure was kept consistent with that during the heating process.

The temperature distribution along the inner top of tube wall (with the mesh on) was measured beforehand under different H_2 pressures of 1, 2, 3, and 4 MPa. The temperature measuring apparatus (see Figure S2-(c)) consisted of six thermocouples (K-type, Φ0.5 mm) with spacings of 1.5, 1.5, 1.0, 1.5, and 1.5 cm; by moving the slider fastened on the fixing device, we were able to measure the temperatures of different positions along the mesh (inner top of the tube wall). The temperature distribution is shown in Figure S3 as a function of distance from the inner surface of the left-hand flange.

Deposits with widths of 2 cm on the mesh corresponding to the inner top part of tube wall were collected for characterization. The as-prepared samples were characterized by powder X-ray diffraction (XRD, Rigaku Miniflex, CuKα) for composition analysis and scanning electron microscopy (SEM, JEOL, JSM-6360LA) for morphology observation. The sample preparation methods for XRD and SEM observations as well as the reusing treatment of the mesh substrate are shown in Figure S2-(b). After collecting the products, the mesh was dipped into an HCl (0.1 mol L^{-1}) solution for several minutes with ultrasonic vibration and washed with distilled water and ethyl alcohol for several times, after which the mesh substrate was finally reused.

Results and discussions

MgH_2/Mg nano/microstructures were synthesized using the hydriding chemical vapor deposition (HCVD) method by controlling the hydrogen pressure and deposition temperature. Figure 1 shows the images of the products, which are inserted in the P-T diagram of MgH_2, deposited on the mesh under different H_2 pressures for a heating time of 7 h. The four samples clearly showed the same boundary at the position of 4.3 ± 0.1 cm distance from the left-hand flange (see Figure S4). By adjusting the temperature distribution (Figure S3), the product images were inserted into the P-T diagram of MgH_2 (Figure 1). On the right side of the boundary (4.3±0.1 cm; line b in Figure 1), which is denoted as area 3 in Figure 1, the samples showed metallic shiny images, especially those deposited at low H_2 pressures; these may be metallic Mg. On the left side of the boundary, the samples showed a white color (area 2 in Figure 1), which can correspond to highly pure MgH_2; however, the samples were black on the low temperature side (area 1 in Figure 1), especially for those prepared at low H_2 pressures, which may indicate low purity of MgH_2. XRD patterns (Figure S5) confirmed these indicators: the metallic shiny substance deposited on the right side of the boundary (area 3 in Figure 1) was Mg, that was partially hydrogenated during the cooling process (in which the H_2 pressures were kept consistent with that in the heating process) after 7 h of heating; these samples showed higher intensity of MgH_2 at high H_2 pressures than that at low pressures. On the left side of the boundary, the white deposits (area 2 in Figure 1) showed highly pure MgH_2, especially those prepared under high H_2 pressures; however, far away from the boundary, at the low temperature side (area 3 in Figure 1), the samples showed decreasing purity of MgH_2 and were black in color (mixture of Mg and MgH_2). This clearly shows that Mg was deposited exactly on the right side of the boundary because MgH_2 is decomposed at higher temperatures, as shown in Figure S1 (the shadowed area). Obviously, highly pure MgH_2 was deposited near the boundary on the left side since thermodynamically it is a stable MgH_2 area. However, a mixture of MgH_2 and Mg was also produced on the low temperature side despite being in the MgH_2 stable area. This is explained later by the hydrogenation kinetics of Mg; the growth mechanism is also discussed.

The measured boundary for the MgH_2 and Mg stable areas is plotted by the red solid line in Figure 1 and compared with the theoretical dissociation pressure for MgH_2, which is the black solid line. The measured boundary showed disagreement with the theoretical pressure as it was shifted to higher temperatures. The measured temperatures for separating the Mg and MgH_2 stable areas at 1, 2, 3, and 4 MPa were 396, 450, 481, and 501 °C, respectively, while the corresponding theoretical temperatures are 387, 427, 454, and 475 °C. Two reasons account for the shift: First, the fluctuation of the temperature distribution along the reactor tube wall caused by H_2 convection;[20] Second, since the products were cooled down to room temperature after several hours of heating while keeping the H_2 pressure constant, the original deposited Mg is partially hydrogenated during the cooling process. However, the measured and theoretical boundaries showed better agreement at the low H_2 pressure of 1 MPa (396 °C and 387 °C, resprectively) than that at high H_2 pressures.

Scanning electron microscopy (SEM) was used to observe the morphology of the as-prepared samples at different H_2 pressures for different deposition temperatures. All of the results are summarized on the P-T diagram of MgH_2 shown in Figures 2 and 3 (Figure 3 is a simplified version of Figure 2; see also Figure S9 for more detailed information). Different shapes of crystals produced at different H_2 pressures and temperatures were classified into six distinct areas: (1) powder-shaped crystals at the nanoscale, where the powders are finer at low temperatures than that at high temperatures; (2) a mixture of powder, dendrite, root-like and curved coarse fibers at the microscale; (3) fiber-shaped crystals, that are curved and straight at the nano/microscale, in which the fibers are straighter and finer at higher pressures; (4) irregular bulk shapes at the microscale; (5) hexagonal shapes at the microscale; and (6) spherical shapes at the microscale.

Until now, we mainly concentrated on the results using a heating time of 7 h to summarize the relationship between the crystal morphology and deposition conditions, i.e. deposition temperature and H_2 pressure. We now demonstrate the kinetics and the growth mechanism here.

Figure 4 shows the images of the products deposited at 2 MPa with different heating times of 7, 13 and 20 h. As confirmed by the XRD analysis shown in Figure 5, prolonging the heating time caused the highly pure MgH_2 product area on the left side of the boundary (4.3 ± 0.1 cm) to shift to a lower temperature (left side). After 20 h of heating, all of the samples showed a single phase of MgH_2; we removed the subsequently deposited metallic shiny materials for 20 h of heating on the white product layer surface and the remaining product on the mesh was used for XRD analysis, which was compared with that of 7 and 13 h of heating; the reason is shown in the latter part about the metallic dendrite Mg crystals. Similar results for samples heated at 1 MPa are shown in the Supporting Information (Figures S6 and S7). Therefore, prolonging the heating time shifts line a in Figures 1 and 3 (only the composition information is considered), or for the boundary of areas 1 and 2, to the low temperature side; this enlarges the MgH_2 deposition area (area 2). This explains why we failed to produce highly pure MgH_2 in area 1 of Figure 1 with a heating time of 7 h, despite it being in the thermodynamically MgH_2 stable area.

The as-proposed gas-gas reaction at the deposition area shown in Eq. (1) should contain the following two steps in series:

$$Mg\,(g) \rightarrow Mg\,(s) \qquad (3) \quad R_1$$

$$Mg\,(s) + H_2\,(g) \leftrightarrow MgH_2\,(s) \qquad (4) \quad R_2$$

Eq. (3) is the condensation of the vaporized Mg, and Eq. (4) is the hydrogenation of the solid Mg. The reaction rates for them are R_1 and R_2, respectively. In the shadowed area of Figure S1 (the Mg stable area), only the condensation of the vaporized Mg occurred because MgH_2 is decomposed at high temperatures, where $R_1 >> R_2$; therefore, we produced Mg at the high temperature condition of area 3 in

Figures 1 and 3. In the white area of Figure S1 (the MgH_2 stable area), the hydrogenation of solid Mg (Eq. (4)) at high temperature and high H_2 pressure conditions had a larger reaction rate than that at low temperature and low H_2 pressure conditions; at the same time, the condensation of the vaporized Mg at low temperature side had a larger reaction rate than that at high temperature side; therefore, at low H_2 pressures of 1 and 2 MPa and at lower temperatures, the products showed a mixture of MgH_2 and Mg, where the reaction rate $R_1 > R_2$ and the solid Mg accumulated. However, prolonging heating time allowed the previously unhydrided Mg to be hydrogenated. The V-S (vapor-solid) growth mechanism was introduced to explain the growth of MgH_2 nanofibers because no catalyst was used during the HCVD process.[21] Combined with the two-step reaction in this study, the shapes of the deposited crystals must be determined by the first step of the Mg condensation. In the V-S mechanism, the shapes of the deposited crystals are affected by the concentration of the source vapor, deposition temperature (concentration of the source vapor and deposition temperature control the supersaturation degree of the source vapor), and deposition cooling rate. Various Mg structures, such as nanowires (curved and straight), spheres, flakes, rods, and sea urchin-like shapes, were successfully prepared by changing the temperature for Mg evaporation and the flow rate of Ar carrier gas in a physical vapor-transport deposition method.[4,5] The vapor source concentration and deposition temperature (and thus different levels of supersaturation) were also found to influence the morphology of MgO grown by the V-S method.[23,24] In our experiments, the Mg raw material was heated to vaporization in the evaporation area at 600 °C under H_2 pressures of 1, 2, 3, and 4 MPa. Two reactions are expected to occur in this area:

$$Mg\,(s) + H_2\,(g) \leftrightarrow MgH_2\,(s) \qquad (5)$$

$$Mg\,(s) \rightarrow Mg\,(g) \qquad (6)$$

Clearly, the concentration of Mg vapor supplied was higher at low H_2 pressures than that at high H_2 pressures. The results showed that in the MgH_2 stable area, a high H_2 pressure and temperature condition was advantageous for producing uniform and thin MgH_2 nanofibers. Fibrous highly pure MgH_2 was produced under 4 MPa H_2 at the temperatures near the theoretical dissociation temperature, where there was a large reaction rate due to a low concentration of Mg vapor and high H_2 pressure; and the reaction rate $R_2 > R_1$, the MgH_2 nanofibers seemed to grow from the direct gas-gas reaction as shown in Eq. (1).

We observed a metallic shiny material deposited on the surface of the white MgH_2 near the boundary of 4.3 ± 0.1 cm at a heating time of 20 h under H_2 pressures of 1 and 2 MPa; the area is indicated by a rectangle in Figure S8. The metallic shiny material had various dendrite shapes similar to the dendrite Mg prepared in our previous study.[21] Due to the long deposition time, the product layer grew thicker, and the temperature on the layer surface was higher than that on the mesh, which may shift to the MgH_2 decomposition area. This is also why the results after 7 h of heating were used to summarize the relationship between the crystal morphology and the deposition conditions for temperature and H_2 pressure.

Conclusions

In summary, we carried out the shape-controlled growth of MgH_2/Mg nano/microstructures by hydriding chemical vapor deposition (HCVD). We were easily able to control the shape of the products by adjusting the deposition temperature and H_2 pressure. The results were plotted on a thermodynamic P-T diagram for MgH_2. Different shapes of crystals having different compositions were prepared at different temperatures and pressures. The growth mechanism for the HCVD method was discussed both thermodynamically and kinetically. The results shown in the P-T diagram will allow us to determine the optimum conditions for synthesizing different shapes of products by HCVD, and this may lay the foundation for the mass production of nano/microsized MgH_2/Mg for use in hydrogen storage or batteries.

Acknowledgements

The authors would like to acknowledge Taiatsu Techno Co. Ltd for their technical support on improving the apparatus. We also thank Mr. G. Saito for his great help during the experiment.

Supporting Information Available: (1) Figure S1: Thermodynamic P-T diagram of MgH_2; (2) Figure S2: Schematic diagram for the preparation of MgH_2/Mg nano/microstructures; (3) Figure S3: Temperature distribution on the mesh at different H_2 pressures; (4) Figure S4: Images of the products deposited on the mesh at different H_2 pressures at a heating time of 7 h; (5) Figure S5: XRD patterns of the samples synthesized at different deposition temperature areas under different H_2 pressures at a heating time of 7 h; (6) Figure S6: Images of the products deposited on the mesh synthesized under 1 MPa H_2 at heating times of 7, 13, and 20 h; (7) Figure S7: XRD patterns of the samples synthesized at different deposition temperature areas under 1MPa H_2 at heating times of 7, 13 and 20 h; (8) Figure S8: Metallic shiny materials separated from the as-deposited white product; (9) Figure S9: Detailed morphology information of the deposited products at different deposition temperatures prepared at different H_2 pressures. This information is available free of charge via the Internet at http://pubs.acs.org/.

REFERENCES

(1) Xia, Y. N.; Yang, P. D.; Sun, Y. G.; Wu, Y. Y.; Mayers, B.; Gates, B.; Yin, Y. D.; Kim, F.; Yan, Y. Q. *Adv. Mater.* **2003**, *15*, 353.

(2) Burda, C.; Chen, X.; Narayanan, R.; El-Sayed, M. A. *Chem. Rev.* **2005**, *105*, 1025.

(3) Lu, J.; Choi, Y. J.; Fang, Z. Z.; Sohn, H. Y.; Rönnebro, E. *J. Am. Chem. Soc.* **2009**, *131*, 15843.

(4) Li, W. Y.; Li, C. S.; Ma, H.; Chen, J. *J. Am. Chem. Soc.* **2007**, *129*, 6710.

(5) Li, W. Y.; Li, C. S.; Zhou, C. Y.; Ma, H.; Chen, J. *Angew. Chem. Int. Ed.* **2006**, *45*, 6009.

(6) Oumellal, Y.; Rougier, A.; Nazri, G. A.; Tarascon, J. M.; Aymard, L. *Nat. Mater.* **2008**, *7*, 916.

(7) Peng, B.; Liang, J.; Tao, Z. L.; Chen, J. *J. Mater. Chem.* **2009**, *19*, 2877.

(8) Stampfer, J. F., Jr.; Holley, C. E., Jr.; Suttle, J. F. *J. Am. Chem. Soc.* **1960**, *82*, 3504.

(9) Schlapbach, L.; Zuttel, A. *Nature* **2001**, *414*, 353.

(10) Aguey-Zinsou, K. F.; Ares-Fernandez, J. R. *Chem. Mater.* **2008**, *20*, 376.

(11) Jongh, P. E. d.; Wagemans, R. W. P.; Eggenhuisen, T. M.; Dauvillier, B. S.; Radstake, P. B.; Meeldijk, J. D.; Geus, J. W.; Jong, K. P. d. *Chem. Mater.* **2007**, *19*, 6052.

(12) Tang, F.; Parker, T.; Li, H. F.; Wang, G. C.; Lu, T. M. *Nanotechnology* **2008**, *19*, 5.

(13) Zlotea, C.; Andersson, Y. *Acta Mater.* **2006**, *54*, 5559.

(14) Zlotea, C.; Lu, J.; Andersson, Y. *J. Alloys Compd.* **2006**, *426*, 357.

(15) Zlotea, C.; Sahlberg, M.; Zbilen, S.; Moretto, P.; Andersson, Y. *Acta Mater.* **2008**, *56*, 2421.

(16) Yao, X. D.; Wu, C. Z.; Du, A. J.; Lu, G. Q.; Cheng, H. M.; Smith, S. C.; Zou, J.; He, Y. H. *J. Phys. Chem. B* **2006**, *110*, 11697.

(17) Yao, X. D.; Wu, C. Z.; Du, A. J.; Zou, J.; Zhu, Z. H.; Wang, P.; Cheng, H. M.; Smith, S.; Lu, G. Q. *J. Am. Chem. Soc.* **2007**, *129*, 15650.

(18) Saita, I.; Toshima, T.; Tanda, S.; Akiyama, T. *Mater. Trans.* **2006**, *47*, 931.

(19) Saita, I.; Toshima, T.; Tanda, S.; Akiyama, T. *J. Alloys Compd.* **2007**, *446-447*, 80.

(20) Matsumoto, I.; Akiyama, T.; Nakamura Y, A. E. *J. Alloys Compd. (In press)*.

(21) Zhu, C.; Hayashi, H.; Saita, I.; Akiyama, T. *Int. J. Hydrogen Energy* **2009**, *34*, 7283.

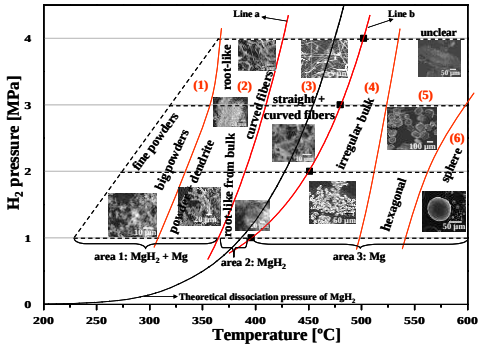
(22) Nakaya U. Snow Crystals, Natural and Artificial. Cambridge: Harvard Univ. Press; 1954. pp. 510.

(23) Yin, Y. D.; Zhang, G. T.; Xia, Y. N. *Adv. Funct. Mater.* **2002**, *12*, 293.

(24) Chen, Y.; Li, J.; Han, Y.; Yang, X.; Dai, J. *J. Cryst. Growth* **2002**, *245*, 163.

For Table of Contents Use Only

Shape-controlled growth of MgH_2/Mg nano/microstructures via hydriding chemical vapor deposition (HCVD) was achieved by adjusting the deposition temperature and H_2 pressure. Different shapes of crystals having different compositions were prepared at different temperatures and pressures. The results were plotted on the thermodynamic P-T diagram of MgH_2, which allows us to determine the optimum conditions for synthesizing different shapes of products by HCVD.



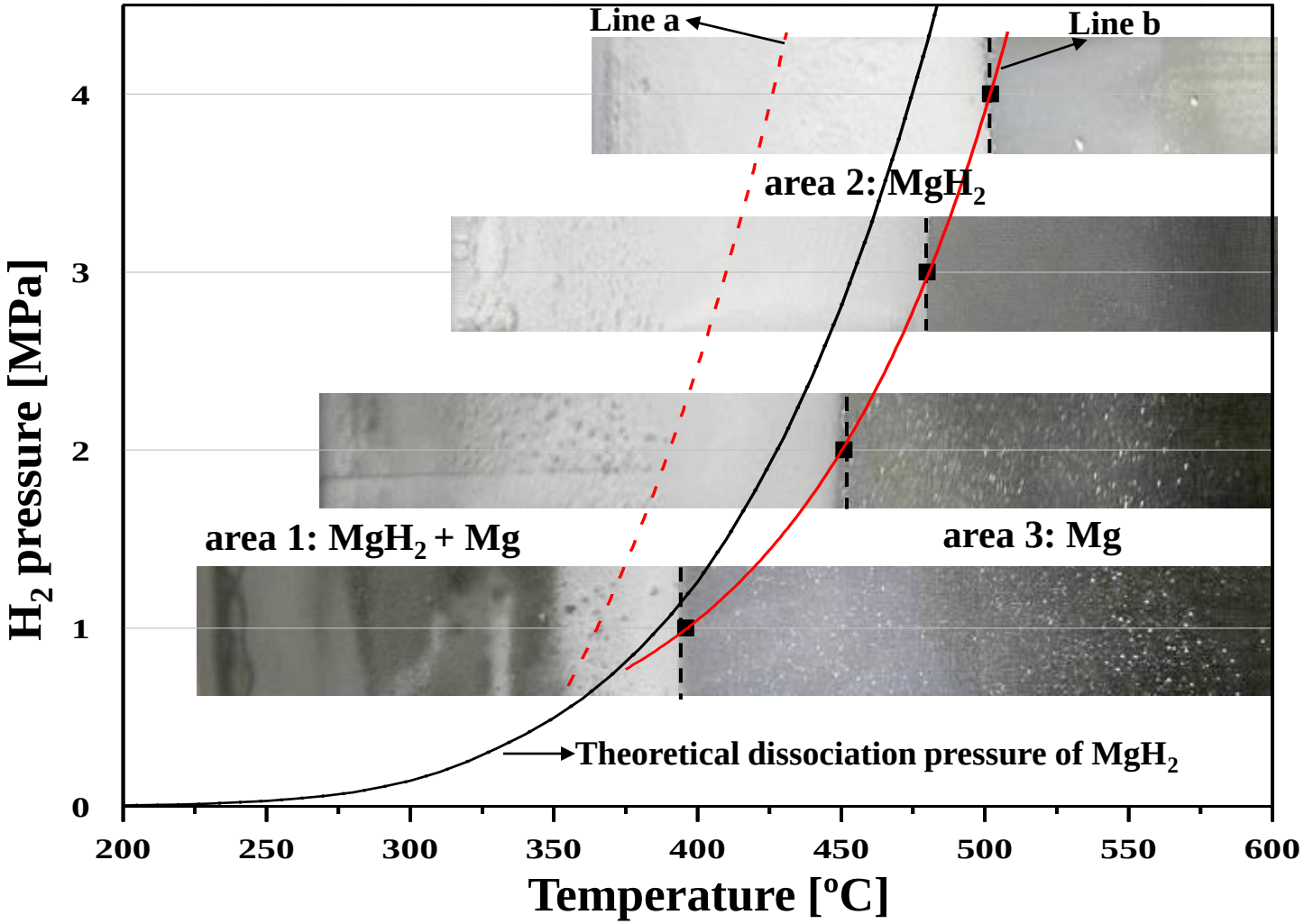

Line a
Line b
area 2: MgH2
area 1: MgH2 + Mg
area 3: Mg
Theoretical dissociation pressure of MgH2
H2 pressure [MPa]
Temperature [°C]
0
1
2
3
4
200
250
300
350
400
450
500
550
600

Figure 1. Deposited product images on the mesh inserted on the P-T diagram of MgH_2. These images were edited to adjust the temperature distribution and sample compositions (more information see Figure S3, Figure S4, and Figure S5). The products were synthesized under H_2 pressures of 1, 2, 3 and 4 MPa, respectively, at a heating time of 7 h. The black solid line is the theoretical dissociation pressure of MgH_2 as a function of temperature, and the red solid line was plotted using the experimental results. Area 1 is a mixture of MgH_2 and Mg; area 2 (between the two red lines) is a highly pure MgH_2 area; and area 3 is Mg. Prolonging the heating time shifts line a to low temperatures (left side) and enlarges the MgH_2 deposition area (area 2).

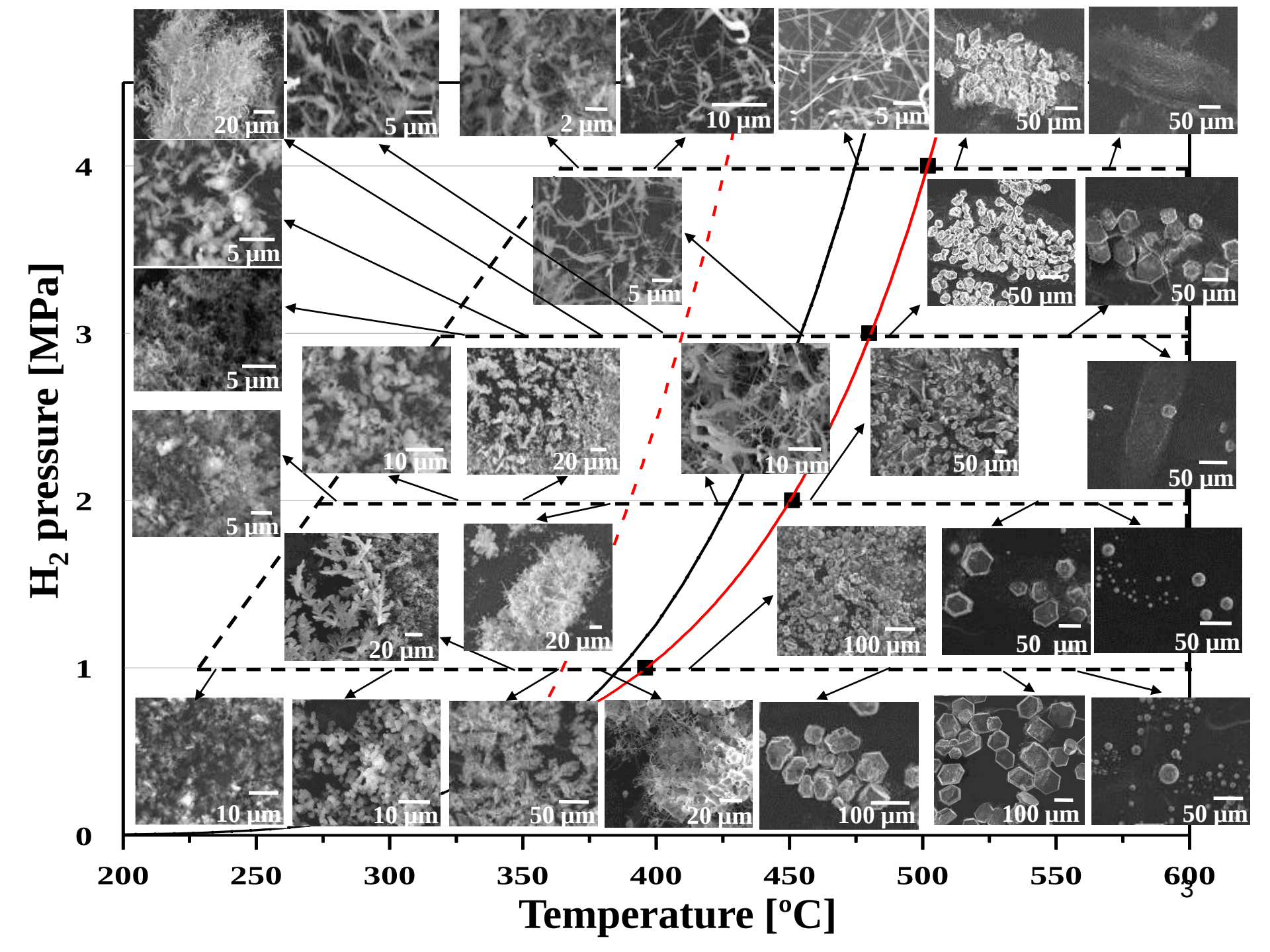

H_2 pressure [MPa]
0
1
2
3
4
200
250
300
350
400
450
500
550
600
Temperature [°C]
20 µm
5 µm
2 µm
10 µm
5 µm
50 µm
50 µm
5 µm
5 µm
50 µm
50 µm
5 µm
10 µm
20 µm
10 µm
50 µm
50 µm
5 µm
20 µm
20 µm
100 µm
50 µm
50 µm
10 µm
10 µm
50 µm
20 µm
100 µm
100 µm
50 µm

Figure 2. Morphology of the deposited products at different deposition temperatures and H_2 pressures inserted on the P-T diagram of MgH_2. The black solid line shows the theoretical dissociation pressure of MgH_2 as a function of temperature. The black dash lines enclose the measurable area in this experiment corresponding to the product images in Figure 1. (More detailed information about the morphology of the deposited products, see Figure S9)

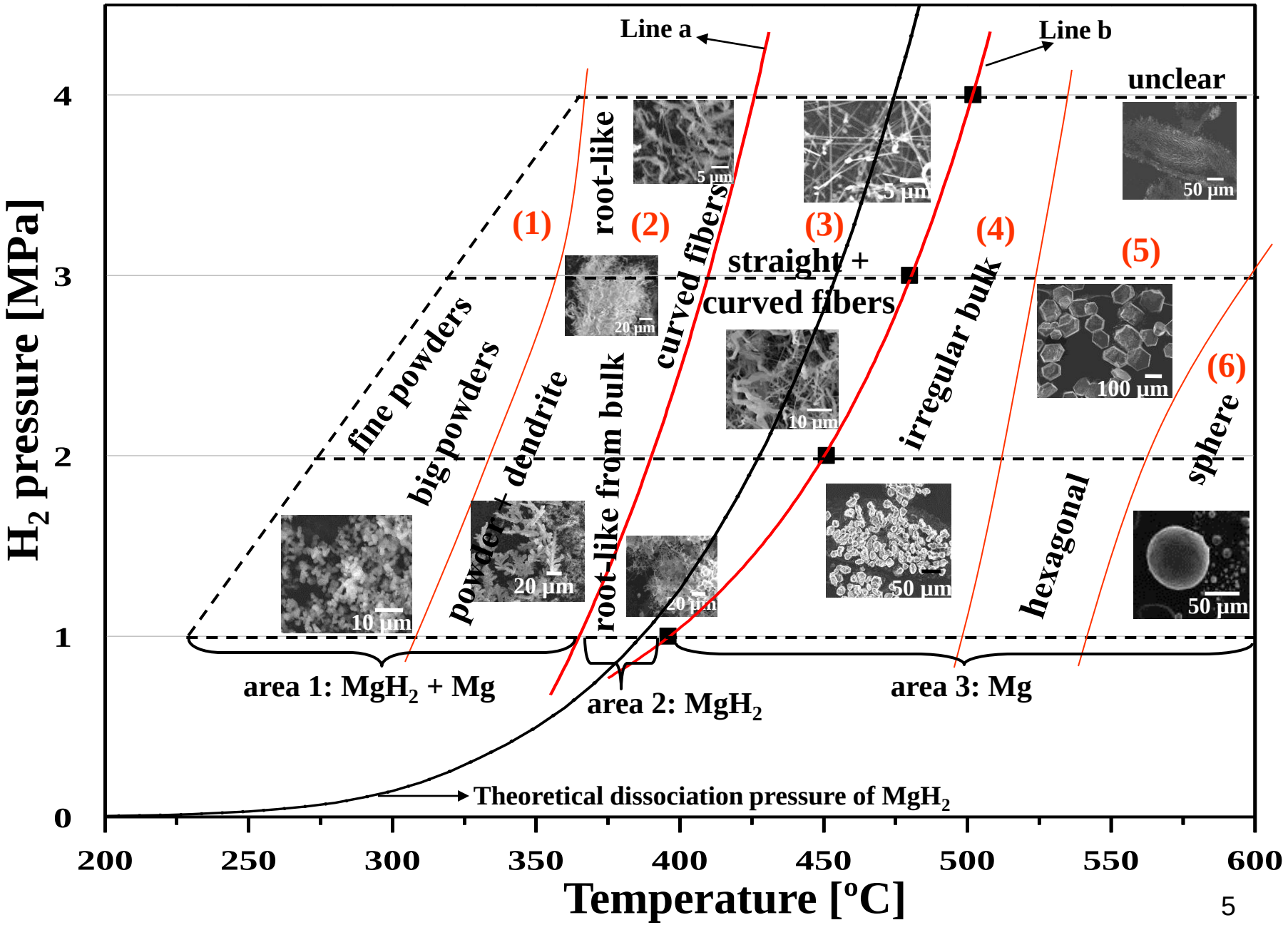

Line a
Line b
unclear
root-like
curved fibers
(1)
(2)
(3)
(4)
(5)
(6)
straight + curved fibers
fine powders
big powders
powder + dendrite
root-like from bulk
irregular bulk
hexagonal
sphere
5 μm
5 μm
50 μm
20 μm
10 μm
100 μm
10 μm
20 μm
20 μm
50 μm
50 μm
area 1: MgH2 + Mg
area 2: MgH2
area 3: Mg
Theoretical dissociation pressure of MgH2
H2 pressure [MPa]
Temperature [°C]
0
1
2
3
4
200
250
300
350
400
450
500
550
600

Figure 3. Simplified morphology and composition distributions of the deposited products at different deposition temperatures and H_2 pressures plotted in the P-T diagram of MgH_2. The composition distribution information is based on the results at a heating time of 7 h. The black solid line shows the theoretical dissociation pressure of MgH_2 as a function of temperature, and line b is plotted using the experimental results. The black dash lines enclose the measurable area in this experiment corresponding to the products images in Figure 1. Area 1 is a mixture of MgH_2 and Mg having powder, dendrite, root-like, and curved fibrous shapes. Area 2 is highly pure MgH_2 having curved and straight fiber shapes. Area 3 is Mg having irregular, hexagonal, and spherical shapes. When only the composition information is considered, prolonging the heating time shifts line a to low temperatures (left side) and enlarges the MgH_2 deposition area (area 2).

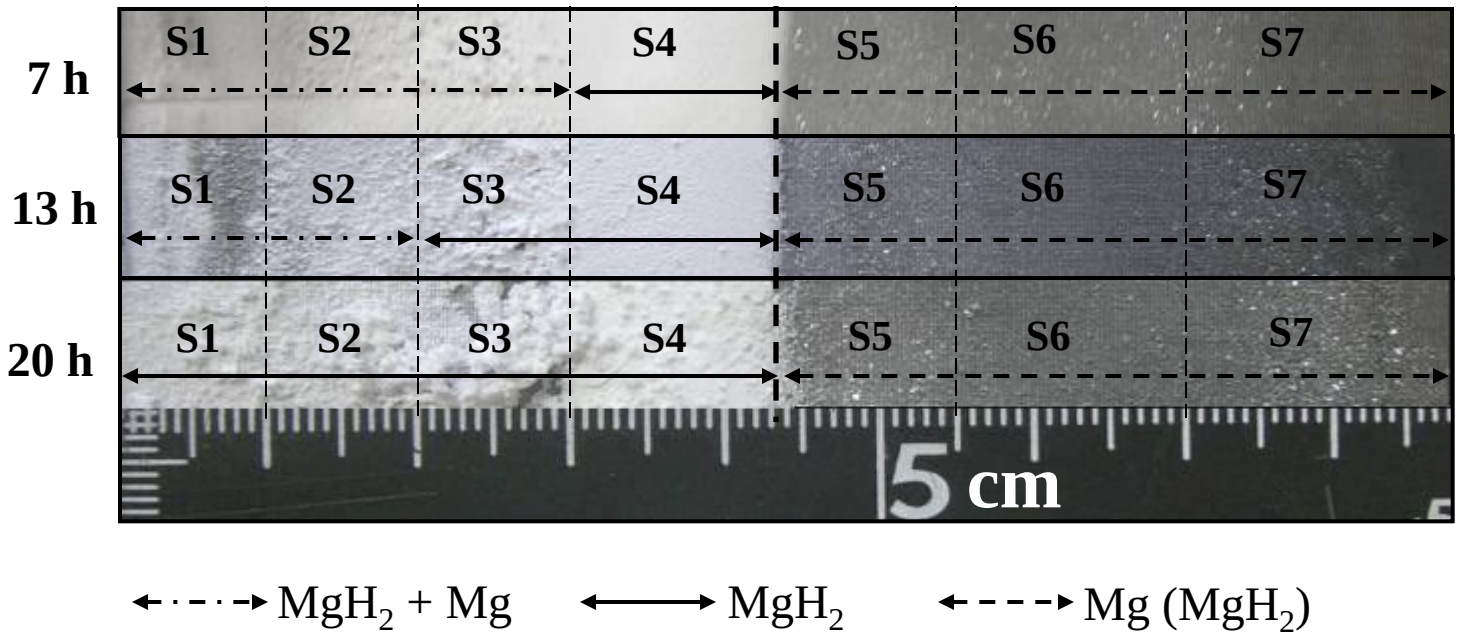


Figure 4. Images of the products deposited on the mesh synthesized under H_2 pressure of 2 MPa at different heating times of 7, 13, and 20 h. Insets show the XRD sample preparation and the composition distribution based on the XRD results in Figure 5.

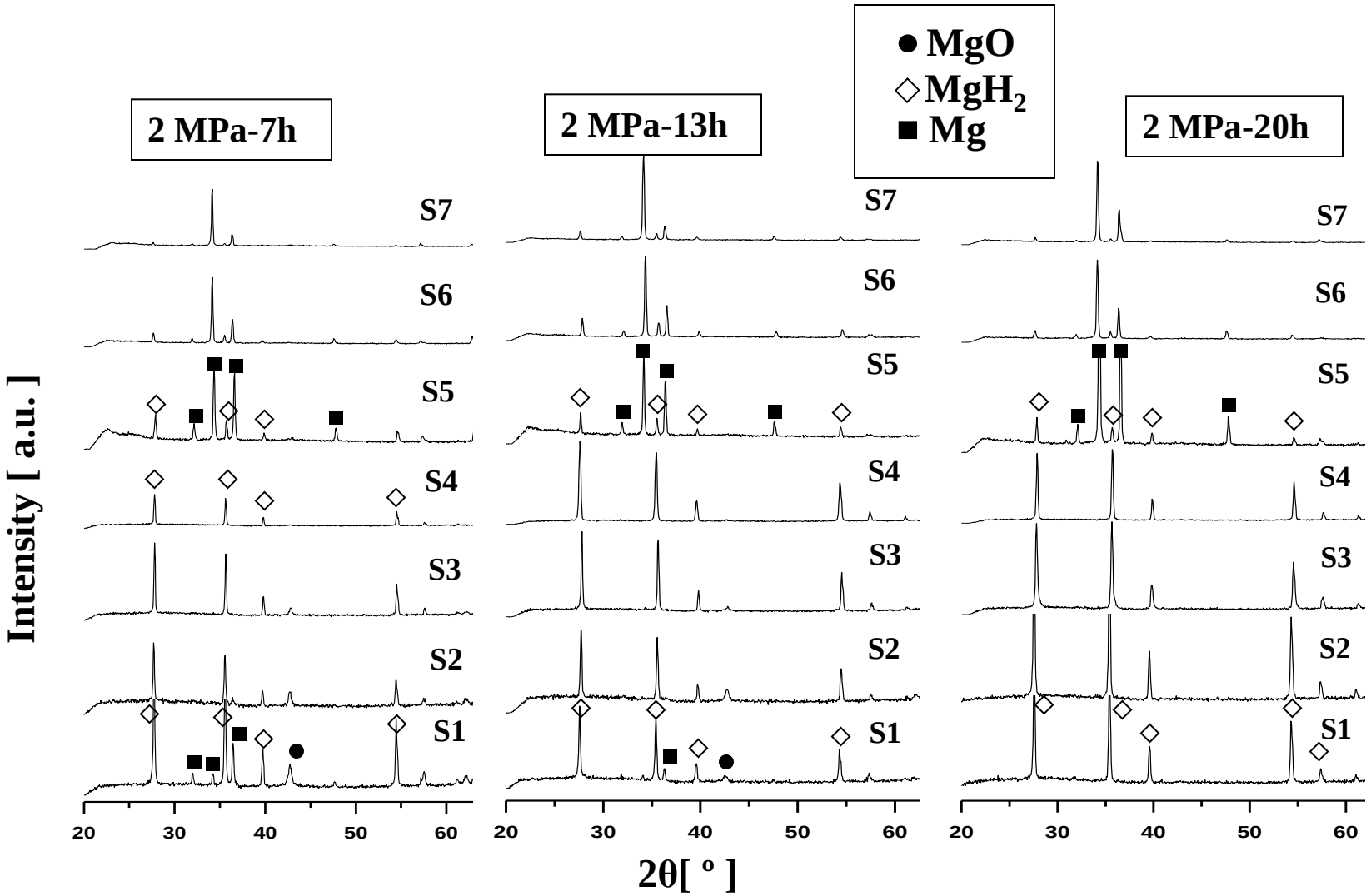


Figure 5. XRD patterns of the samples synthesized at different deposition temperature areas under 2 MPa of H_2 at heating times of 7, 13 and 20 h. The sample numbers correspond to that in Figure 4. MgO peaks were due to exposure of the samples to the air during measuring, and the unhydrogenated Mg was partially oxidized.

Supporting information

Shape-controlled Growth of MgH_2/Mg Nano/Microstructures via Hydriding Chemical Vapor Deposition

Chunyu Zhu † *Sou Hosokai,* † *Itoko Matsumoto,* ‡ *Tomohiro Akiyama,* *†

† Center for Advanced Research of Energy Conversion Materials, Hokkaido University, Sapporo 060-8628, Japan
‡ Energy Technology Research Institute, National Institute of Advanced Industrial Science and Technology, Ibaraki 305-8565, Japan
* Corresponding author, Tel.: +81-11-706-6842; Fax: +81-11-726-0731.
Email: takiyama@eng.hokudai.ac.jp

Contents:

(1) Figure S1: Thermodynamic P-T diagram of MgH_2
(2) Figure S2: Schematic diagram for the preparation of MgH_2/Mg nano/microstructures
(3) Figure S3: Temperature distribution on the mesh at different H_2 pressures
(4) Figure S4: Images of the products deposited on the mesh at different H_2 pressures at a heating time of 7 h
(5) Figure S5: XRD patterns of the samples synthesized at different deposition temperature areas under different H_2 pressures at a heating time of 7 h
(6) Figure S6: Images of the products deposited on the mesh synthesized under 1 MPa H_2 at heating times of 7, 13, and 20 h
(7) Figure S7: XRD patterns of the samples synthesized at different deposition temperature areas under 1MPa H_2 with heating times of 7, 13, 20 h
(8) Figure S8: Metallic shiny materials separated from the as-deposited white product
(9) Figure S9: Detailed morphology information of the deposited products at different deposition temperatures prepared at different H_2 pressures

(1).

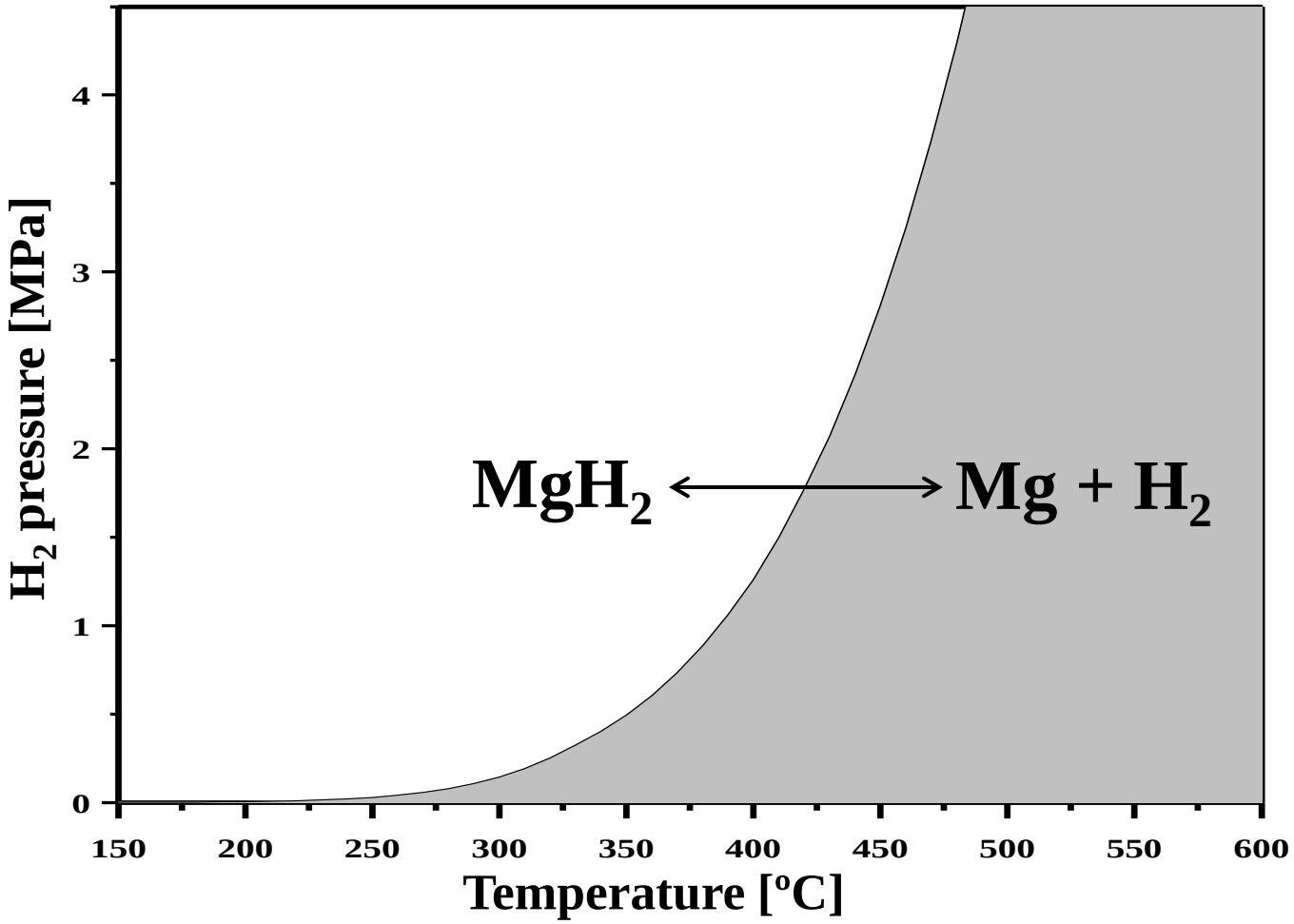
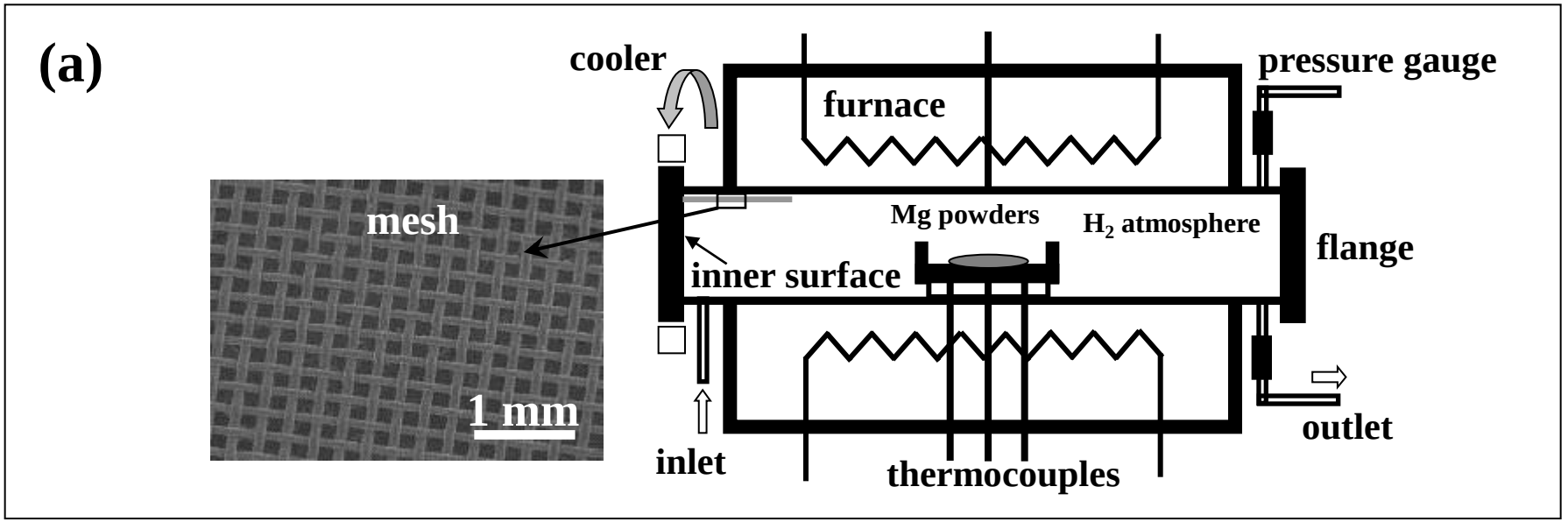


Figure S1. Thermodynamic P-T diagram of MgH_2 (Dissociation pressure of MgH_2 as a function of temperature). This diagram is calculated using HSC Chemistry, Version 5.1, based on the dissociation of MgH_2: MgH_2 (s) ↔ Mg (s) + H_2 (g).

(2).


(a)
cooler
pressure gauge
furnace
mesh
1 mm
Mg powders
H_2 atmosphere
flange
inner surface
outlet
inlet
thermocouples
(b)
washing
cooler
mesh
0.1M HCl
ultrasonic bath
sticky carbon tape
SEM/XRD sample stage
flange
inner surface
SEM observation
XRD characterization
inlet
product on mesh
mesh

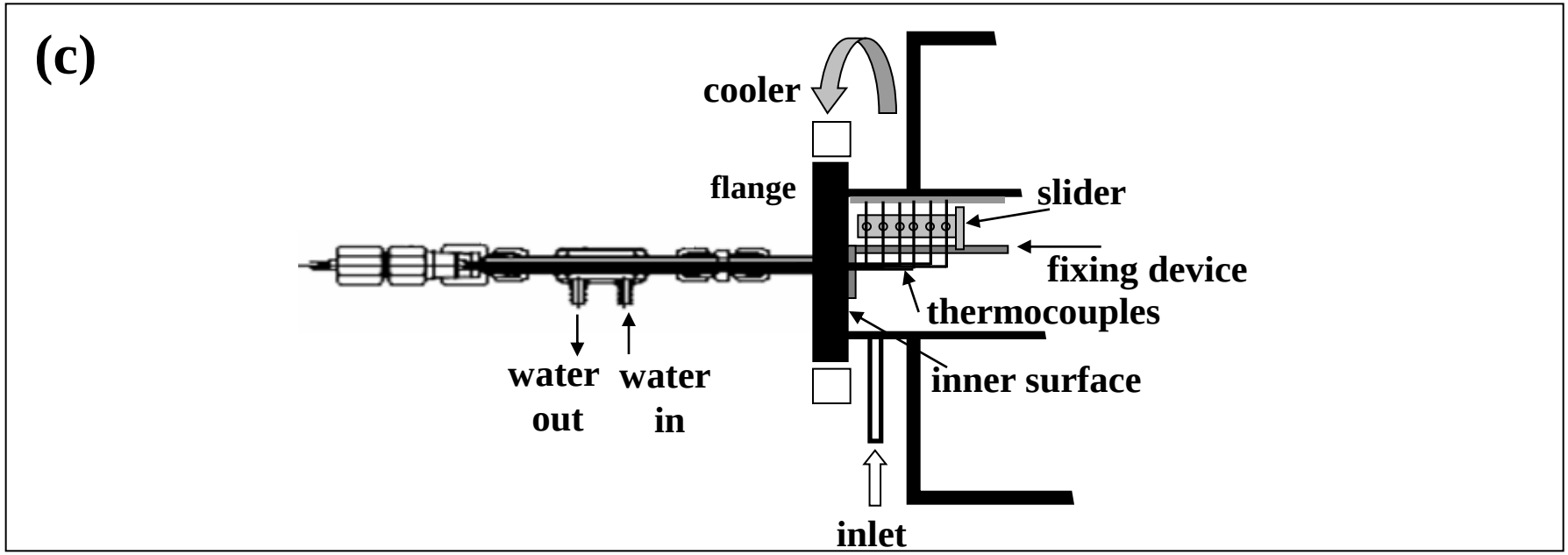


Figure S2. (a) Schematic diagram of the whole experimental setup with the enlarged stainless mesh used;

(b) Schematic diagram of the preparation methods for XRD and SEM observations as well as the reusing treatment of the mesh substrate.

(c) Schematic diagram of the temperature measuring setup.

(3).

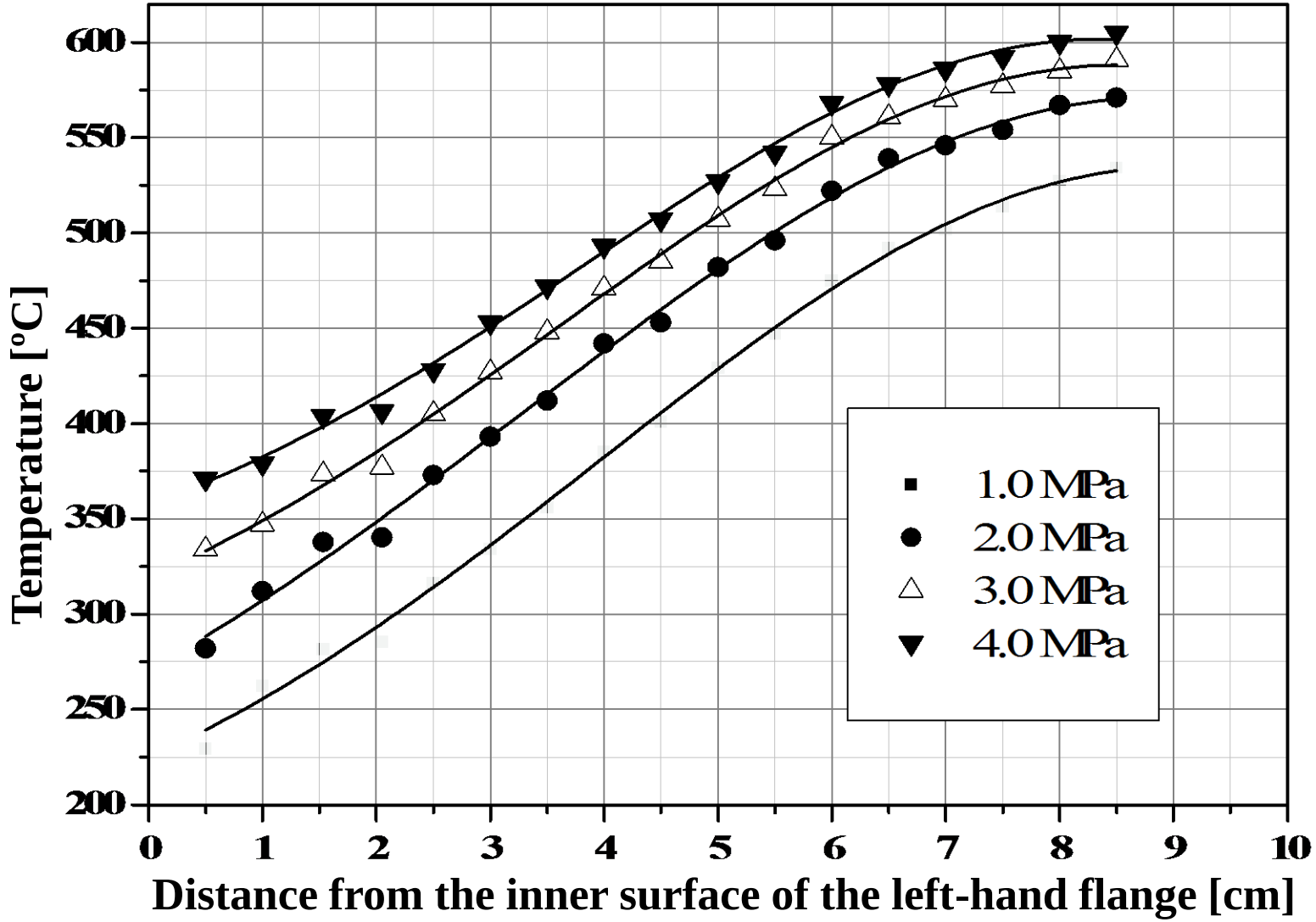


Figure S3. Temperature distribution on the mesh adhered along the tube wall under H_2 pressures of 1.0, 2.0, 3.0, and 4.0 MPa, respectively. The top of tube with the mesh on was measured.

(4).

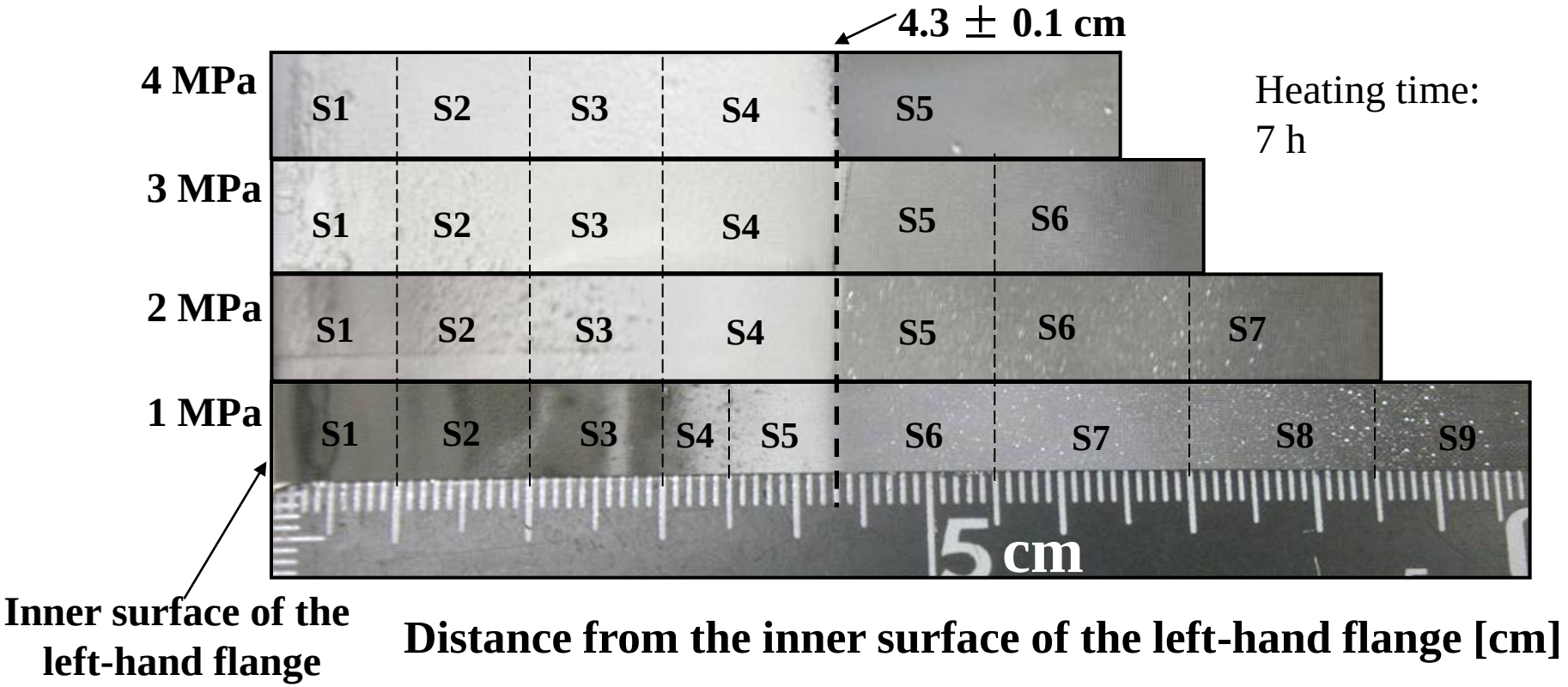
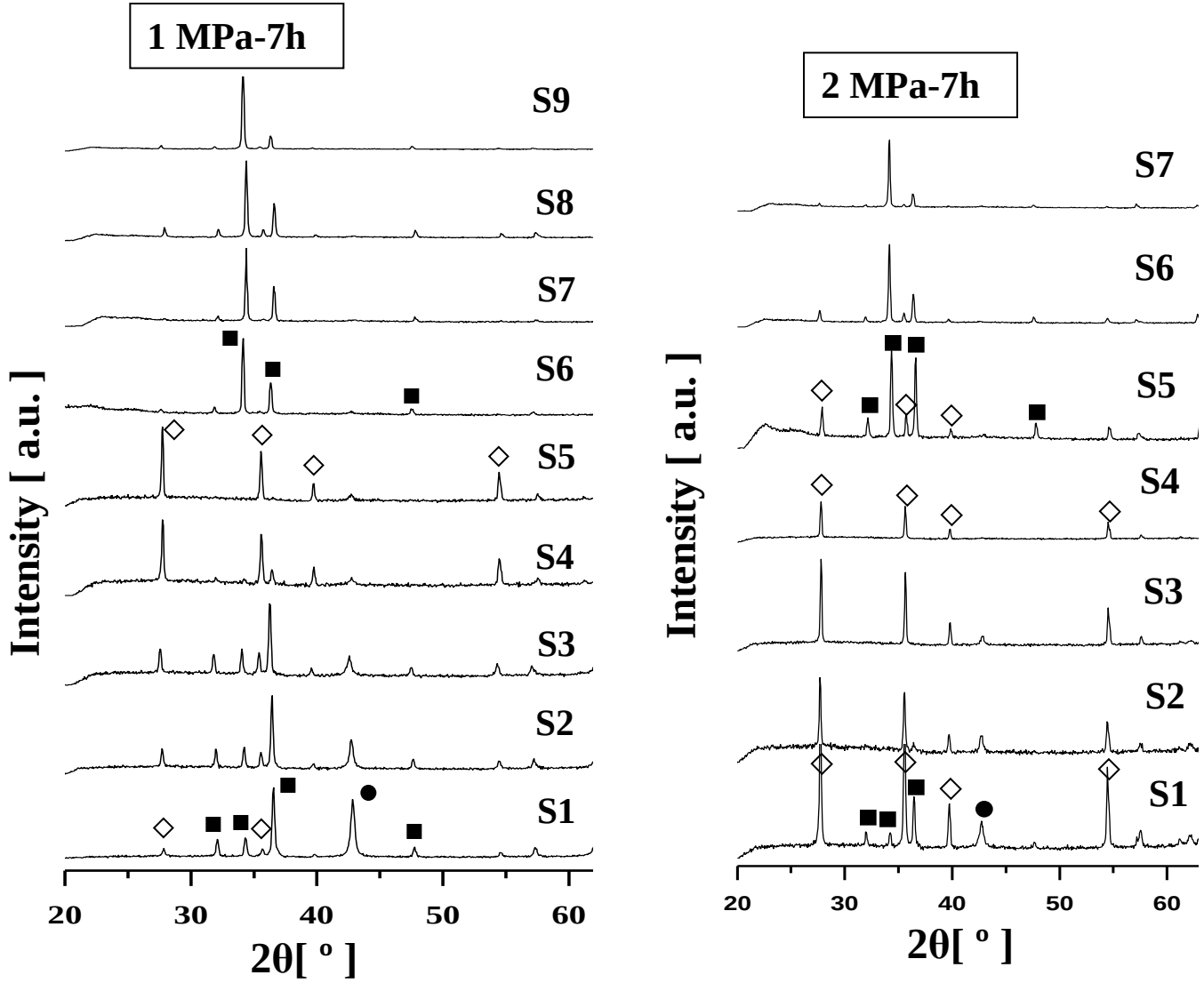


Figure S4. Images of the products deposited on the mesh under H_2 pressures of 1, 2, 3, and 4 MPa, respectively, at a heating time of 7 h. Insets show the XRD samples preparation. The deposits on the mesh corresponding to the central top of the tube wall were collected.

(5).


1 MPa-7h
S9
S8
S7
S6
S5
S4
S3
S2
S1
Intensity [a.u.]
20
30
40
50
60
2θ[º]
2 MPa-7h
S7
S6
S5
S4
S3
S2
S1
Intensity [a.u.]
20
30
40
50
60
2θ[º]

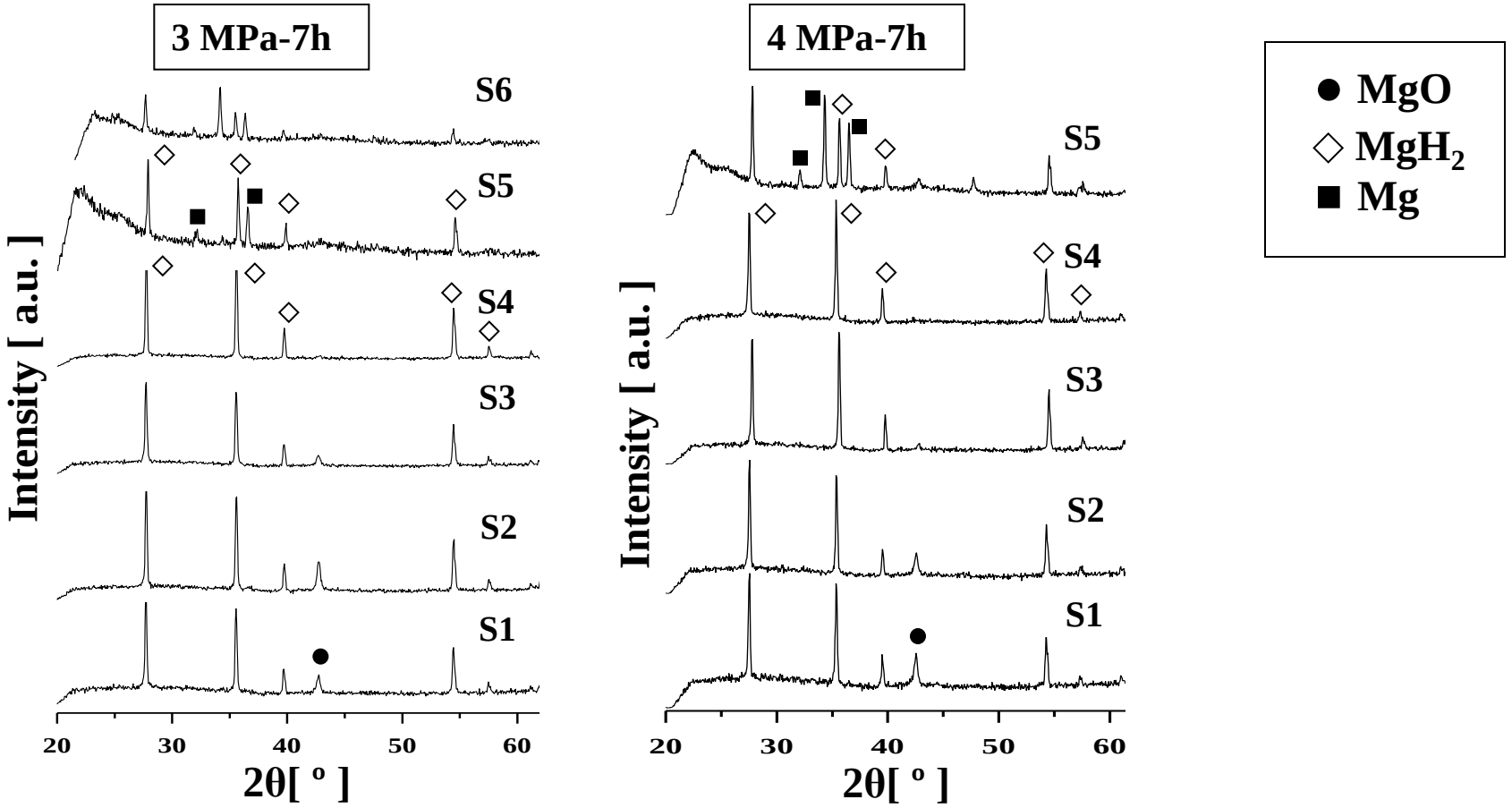


Figure S5. XRD patterns of the samples synthesized at different deposition temperature areas under 1, 2, 3, and 4 MPa of H_2, respectively, at a heating time of 7 h; the sample numbers correspond to that in Figure S4. The peaks of MgO appeared in the XRD patterns, this is due to the exposure of these samples to the air, and the unhydrided Mg was partially oxidized, especially in the low deposition temperature and low H_2 pressure areas where the deposited products were fine powders.

(6).

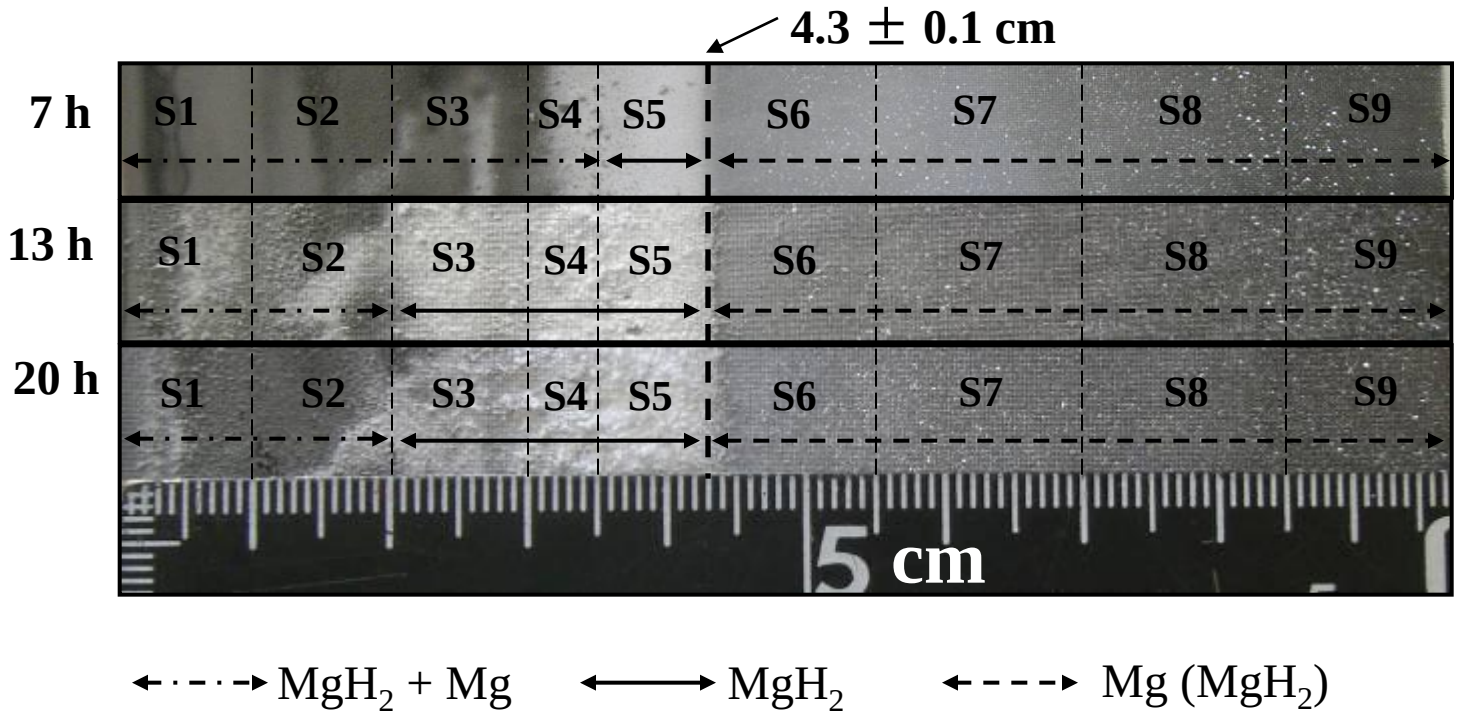


Figure S6. Images of the products deposited on the mesh synthesized under H_2 pressure of 1 MPa at different heating times of 7, 13, and 20 h. Insets show the XRD samples preparation and the composition distribution based on the XRD results in Figure S7.

More discussion about the results under H_2 pressure of 1 MPa can be found in "Chunyu Zhu et al., Investigation of MgH_2 production at low H_2 pressure via hydriding chemical vapor deposition. *Proceeding of Renewable Energy 2010*, Yokohama, Japan."

(7).

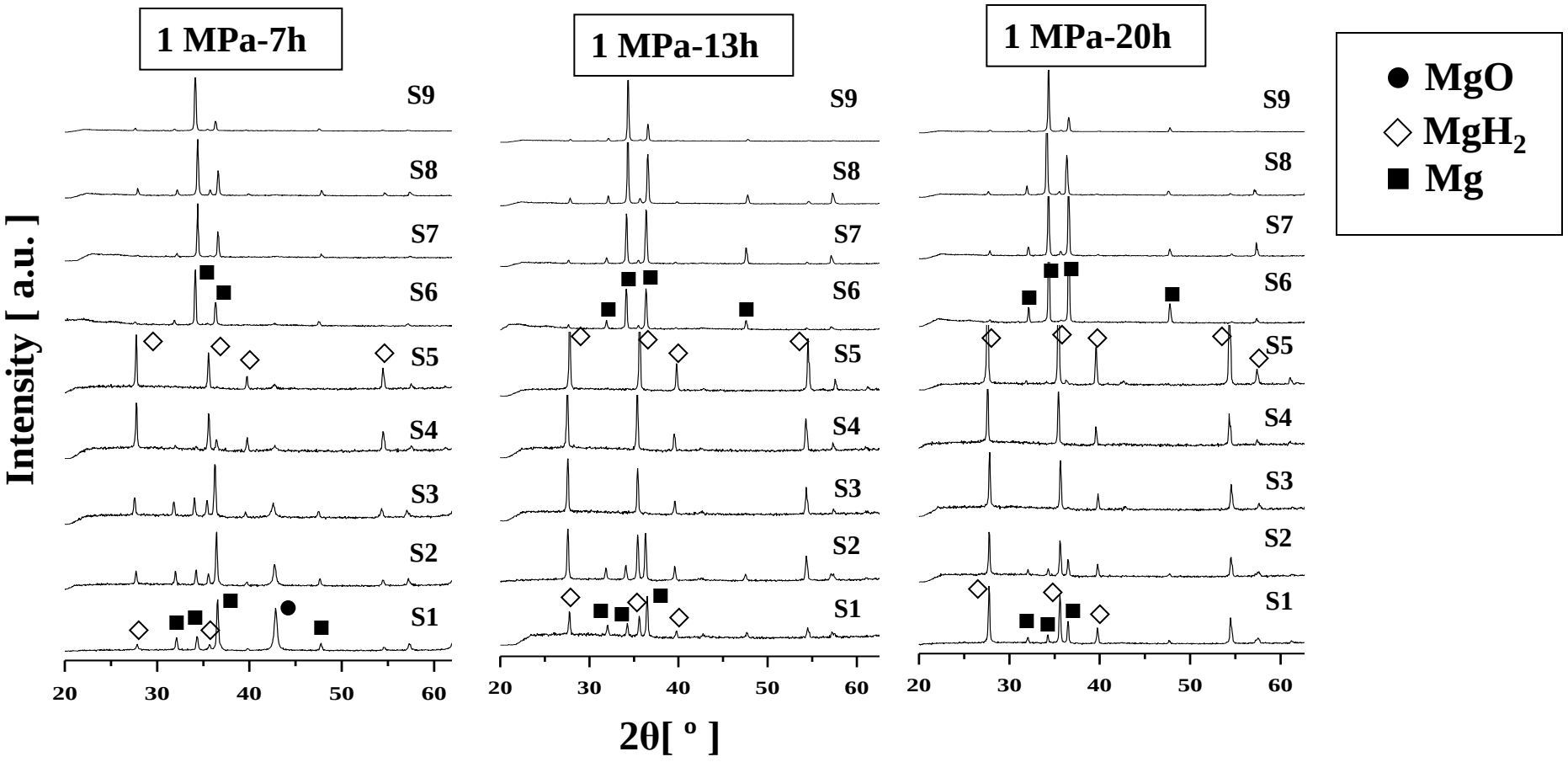


Figure S7. XRD patterns of the samples synthesized at different deposition temperature areas under 1 MPa of H_2 with heating times of 7, 13, and 20 h. The sample numbers correspond to that in Figure S6. MgO peaks were due to exposure of the samples to the air during measuring.

(8).

Metallic shiny Mg deposited under 1 MPa with a heating time of 20 h

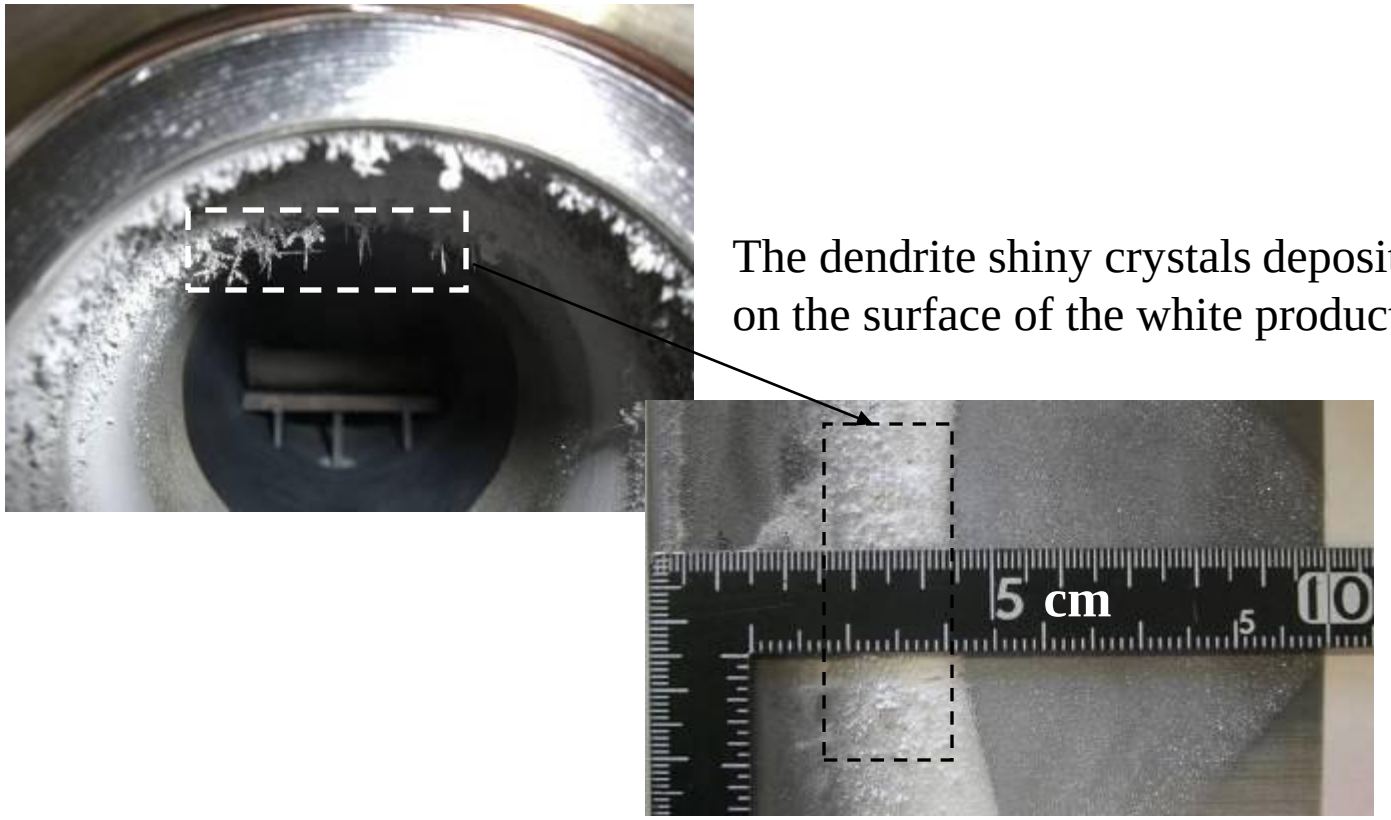
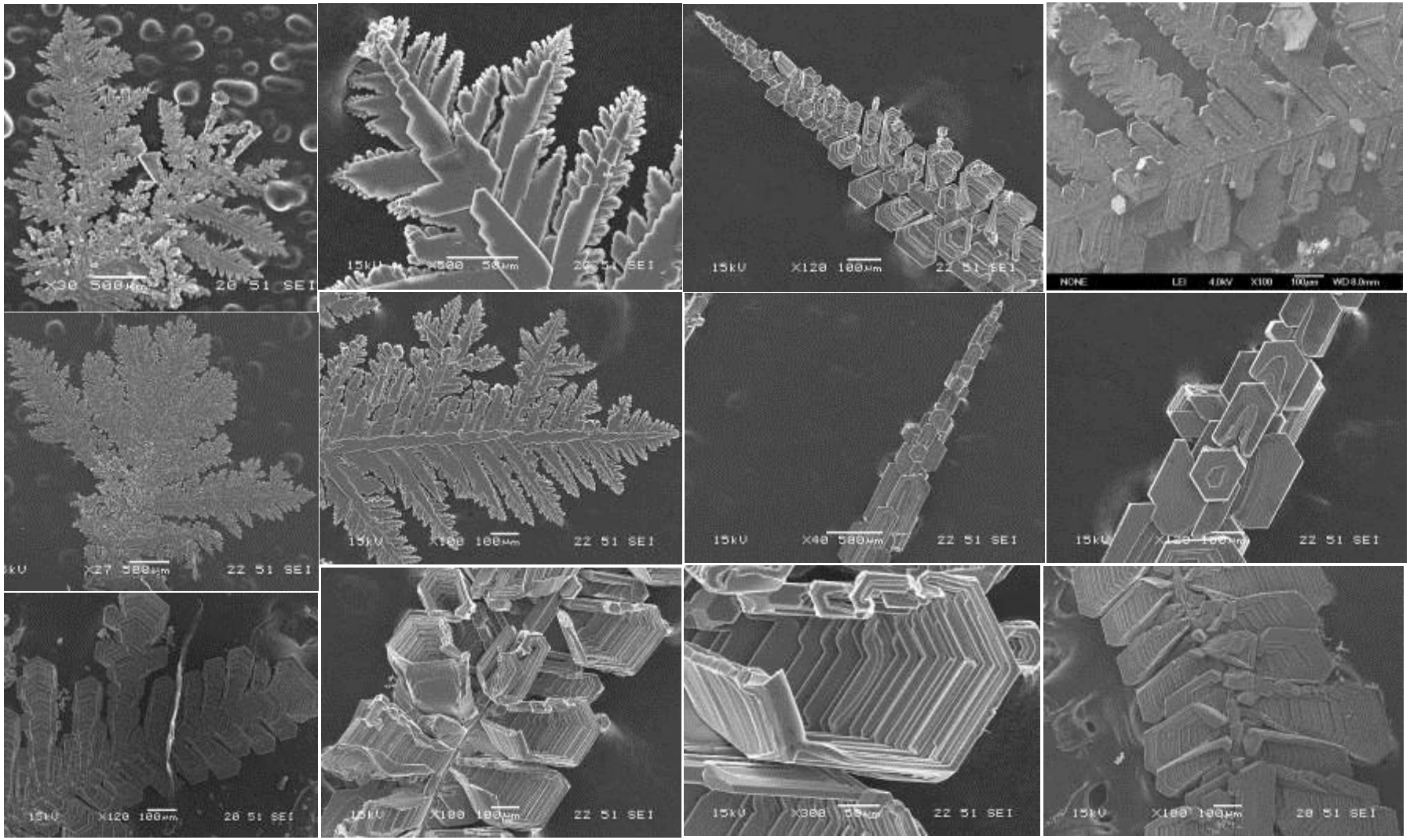


Figure S8. Metallic shiny materials separated from the as-deposited white product (MgH_2) near the boundary of 4.3 ± 0.1 cm. The heating time was 20 h at 1 MPa H_2. The one at 2 MPa with heating time of 20 h have the similar dendrite crystals.

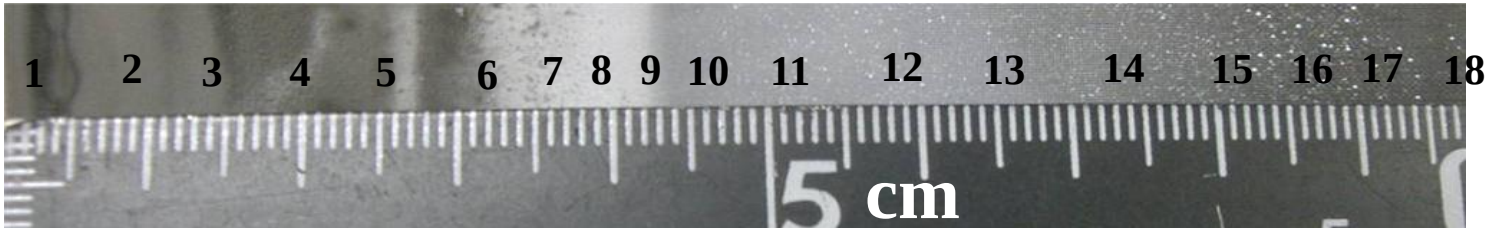
SEM images of the metallic shiny material



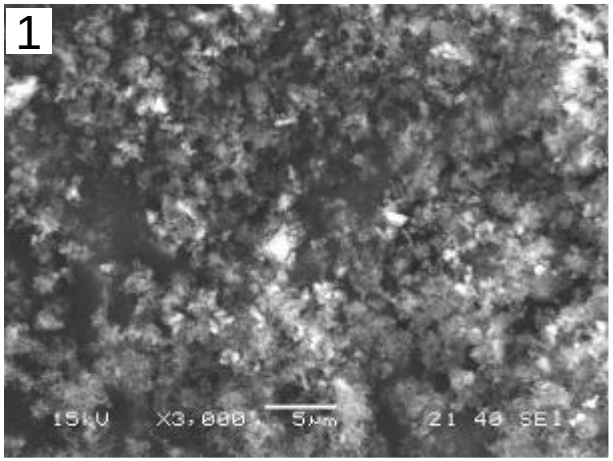
(9).

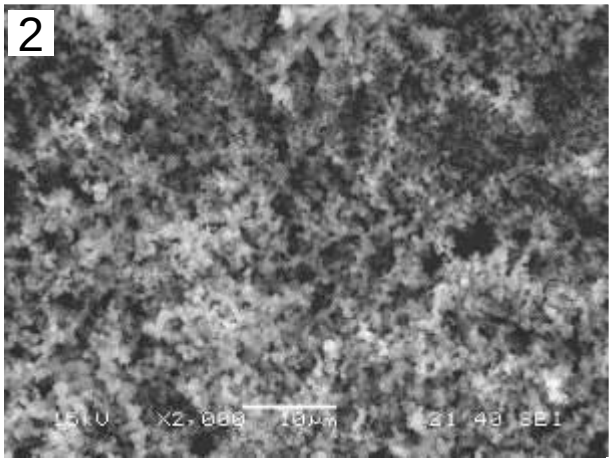
Figure S9. Detailed morphology information of the deposited products at different deposition temperatures prepared at different H_2 pressures.

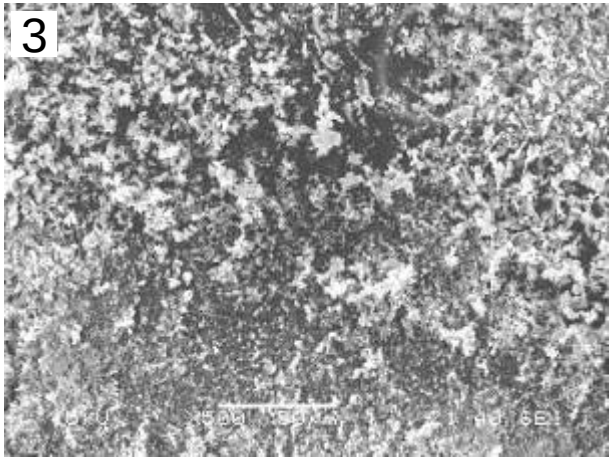
1 MPa-product image

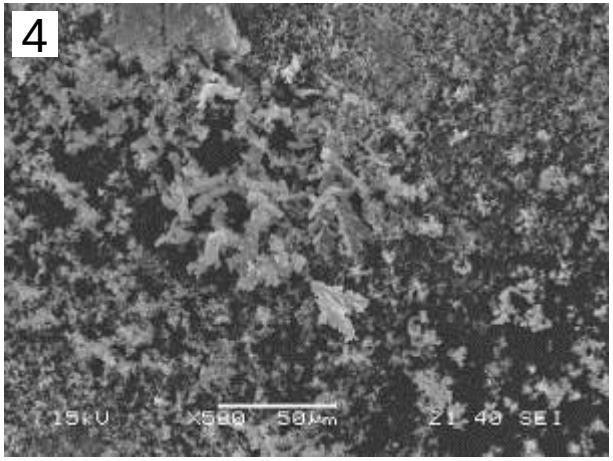


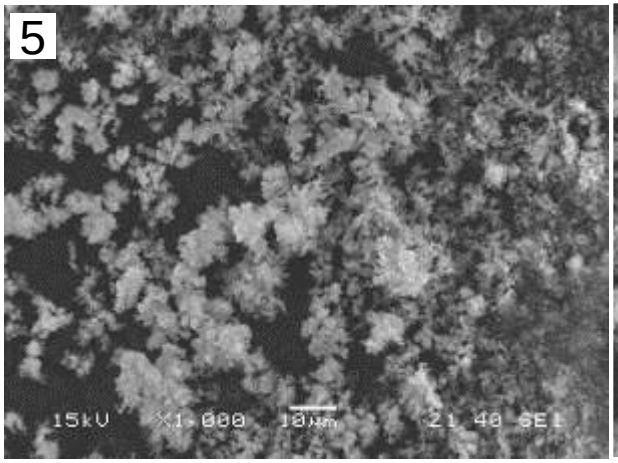
1 MPa-SEM

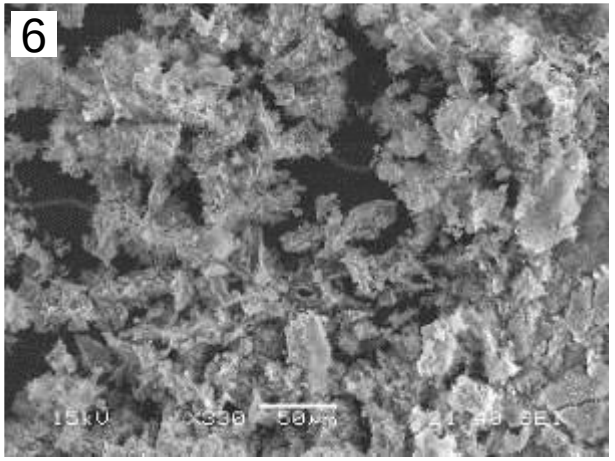

1
15kV X3,000 5μm 21 40 SEI

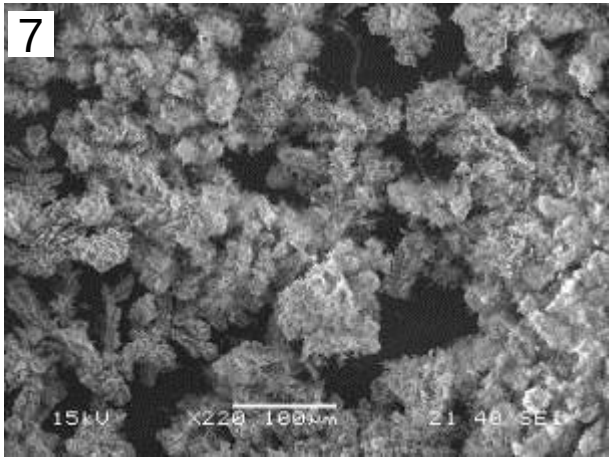

2
15kV X2,000 10μm 21 40 SEI

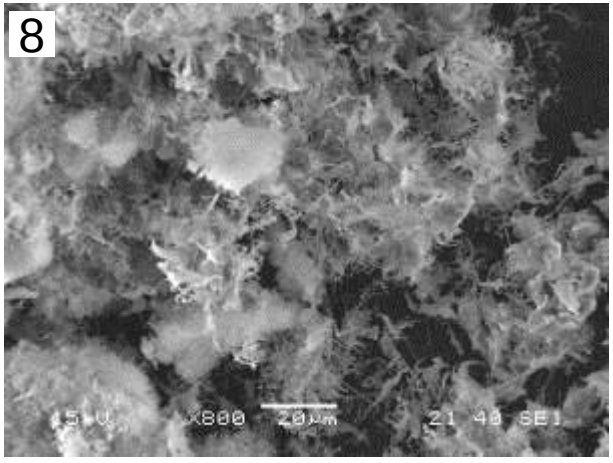

3

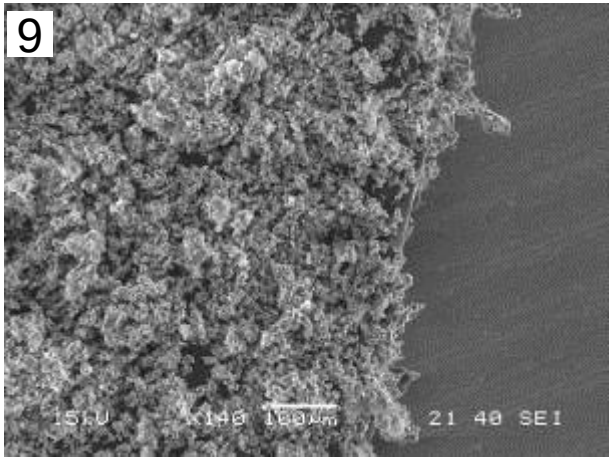

4
15kV X500 50μm 21 40 SEI


5
15kV X1,000 10μm 21 40 SEI

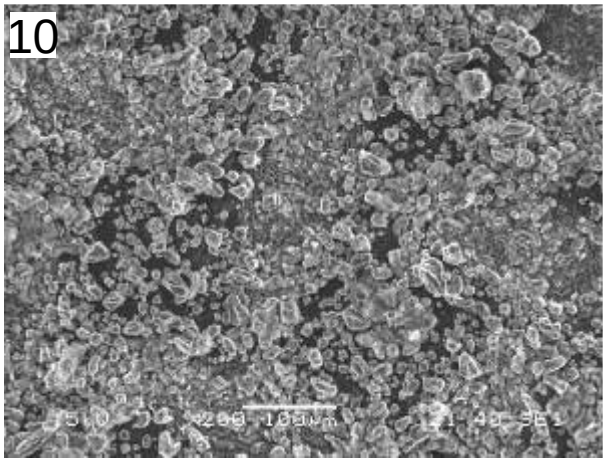

6
15kV X330 50μm 21 40 SEI

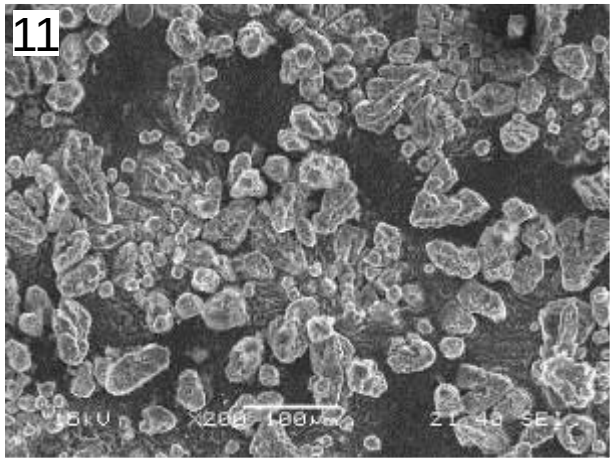

7
15kV X220 100μm 21 40 SEI

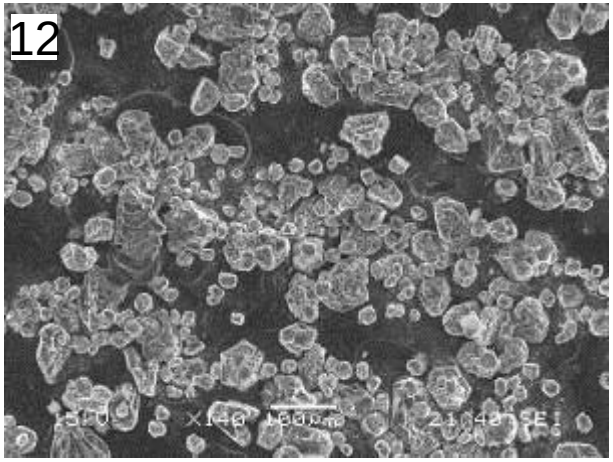

8
15kV X800 20μm 21 40 SEI

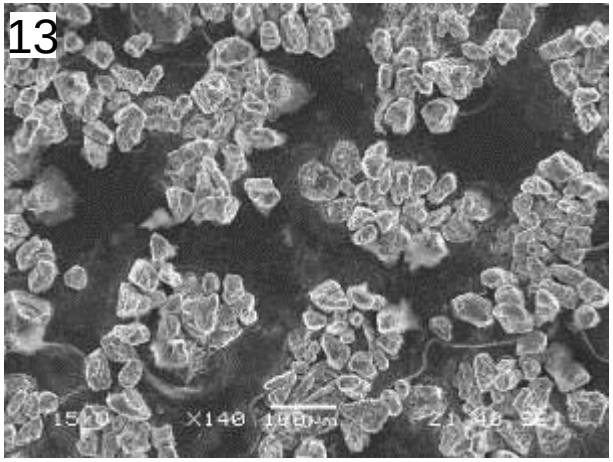

9
15kV X140 100μm 21 40 SEI

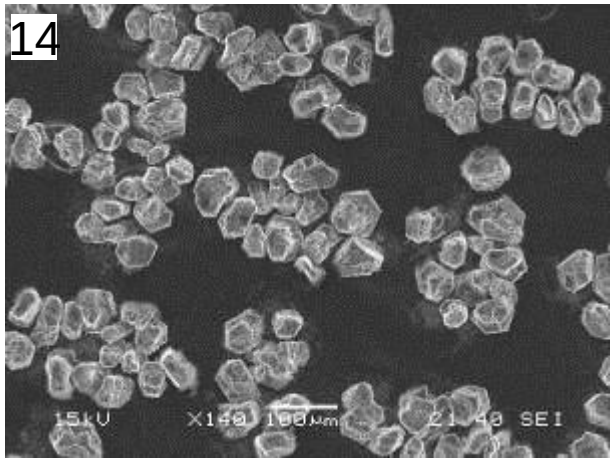
1 MPa-SEM

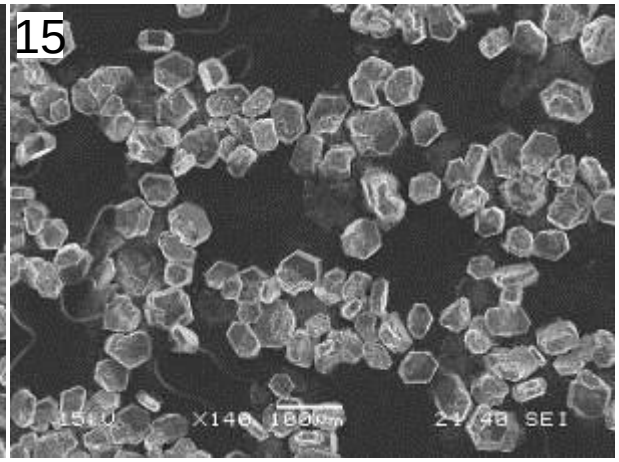


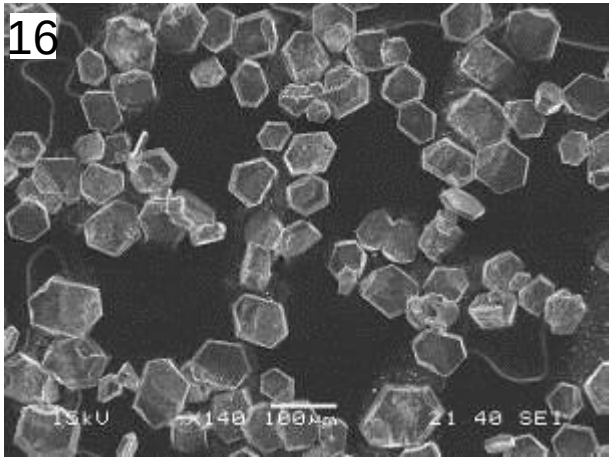


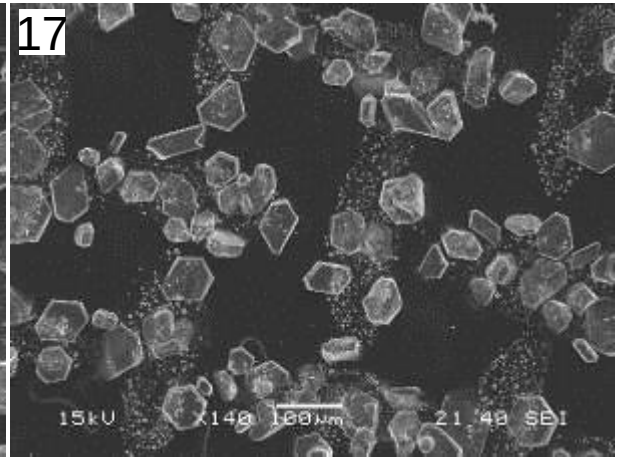


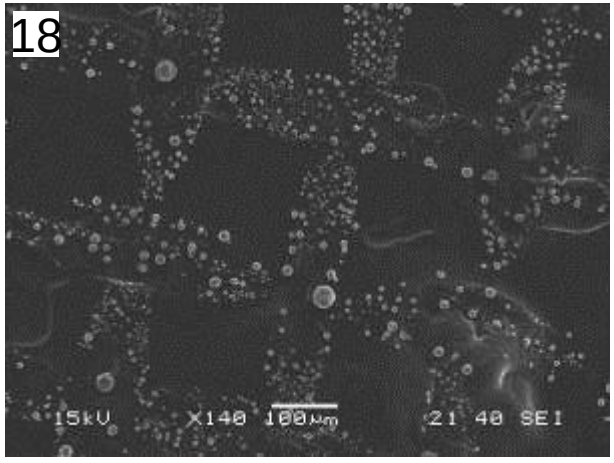




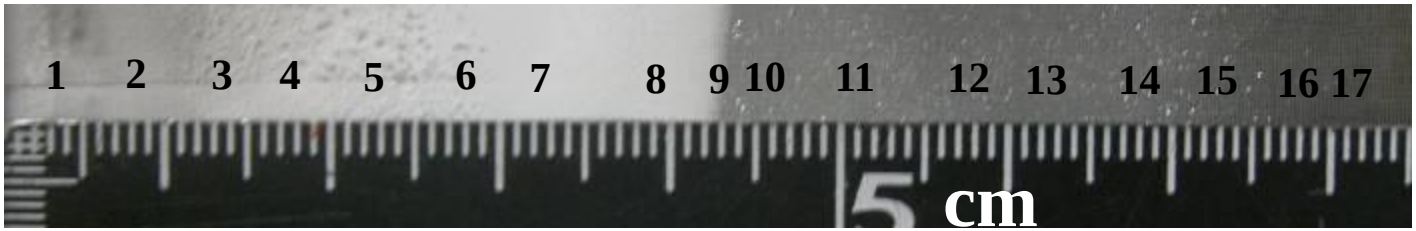




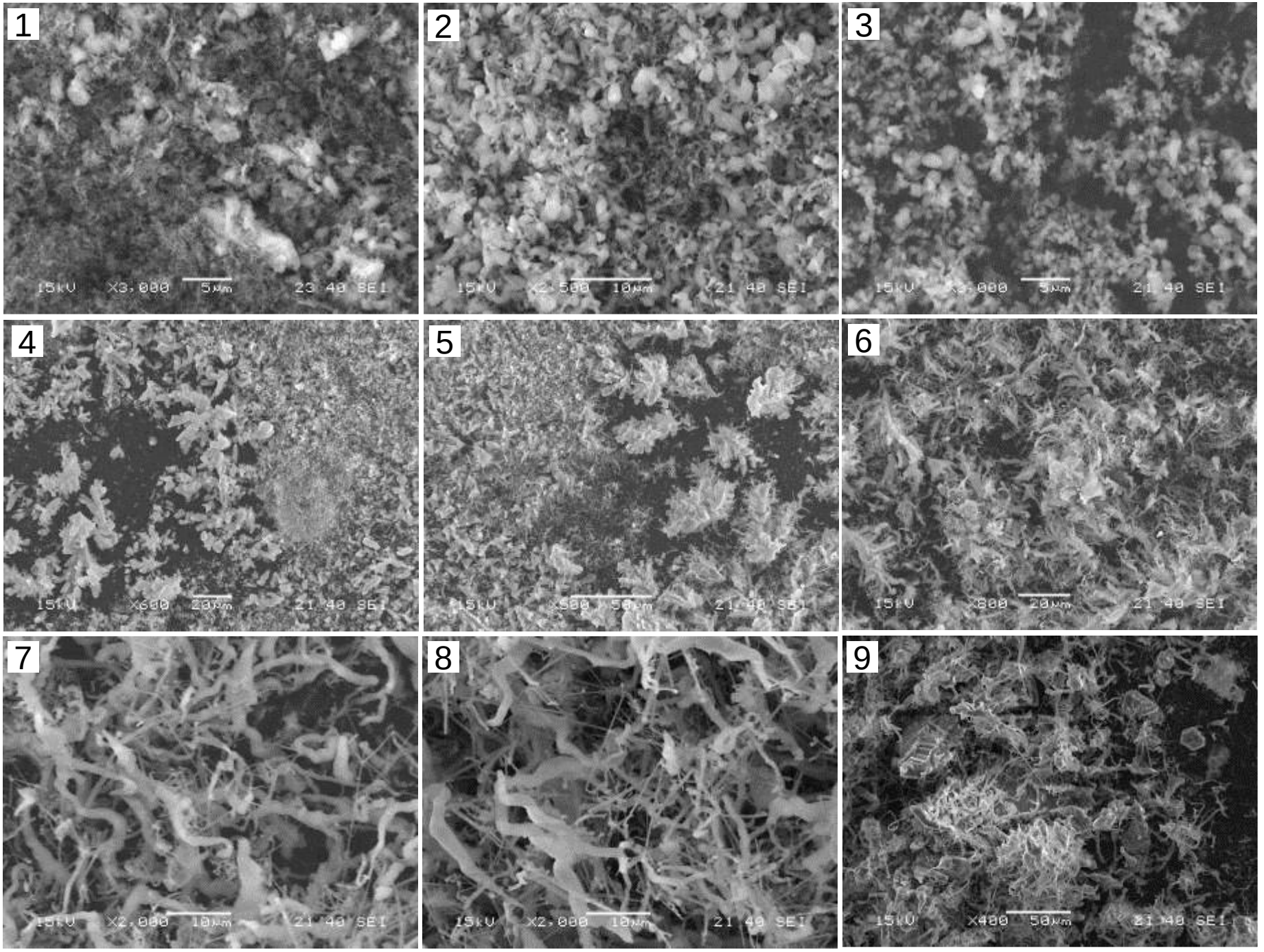




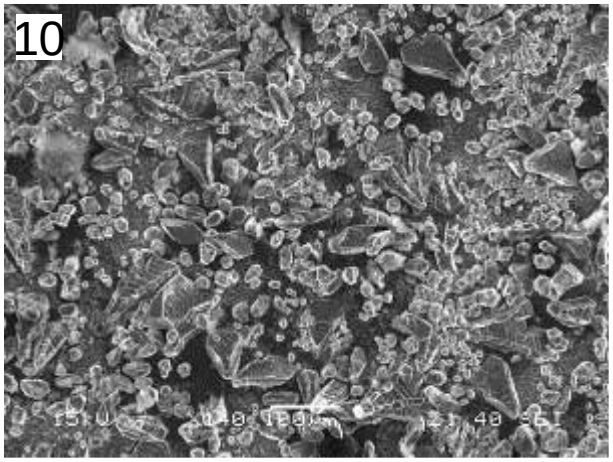
2 MPa-product image

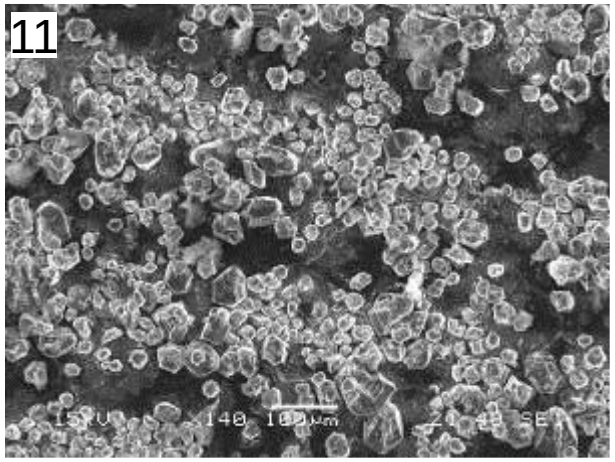


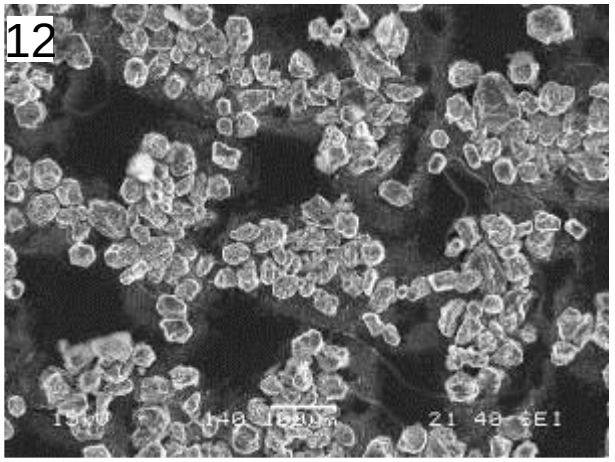
2 MPa-SEM

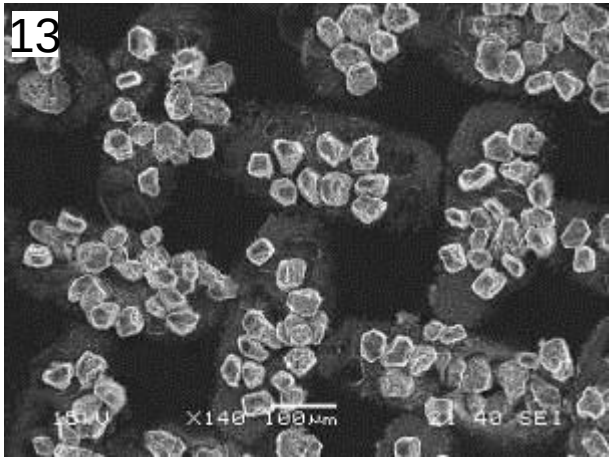

1
15kV X3,000 5μm 23 40 SEI
2
15kV X2,500 10μm 21 40 SEI
3
15kV X3,000 5μm 21 40 SEI
4
15kV X600 20μm 21 40 SEI
5
15kV X500 50μm 21 40 SEI
6
15kV X800 20μm 21 40 SEI
7
15kV X2,000 10μm 21 40 SEI
8
15kV X2,000 10μm 21 40 SEI
9
15kV X400 50μm 21 40 SEI

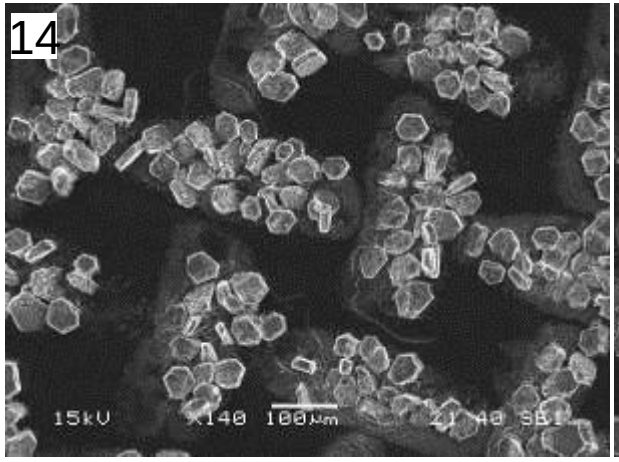
2 MPa-SEM

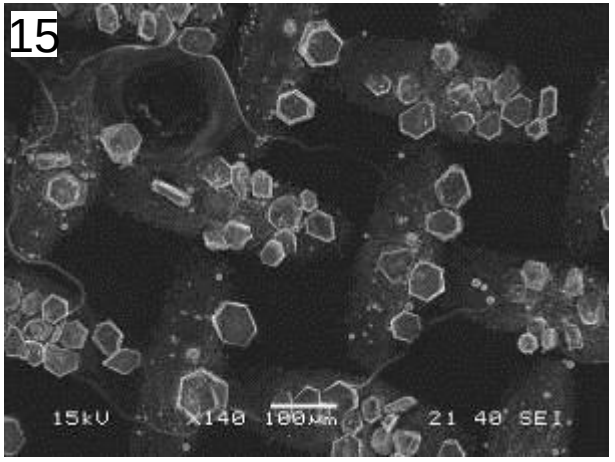


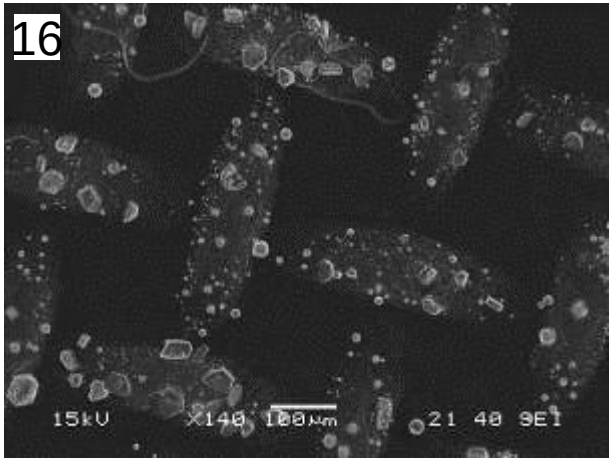


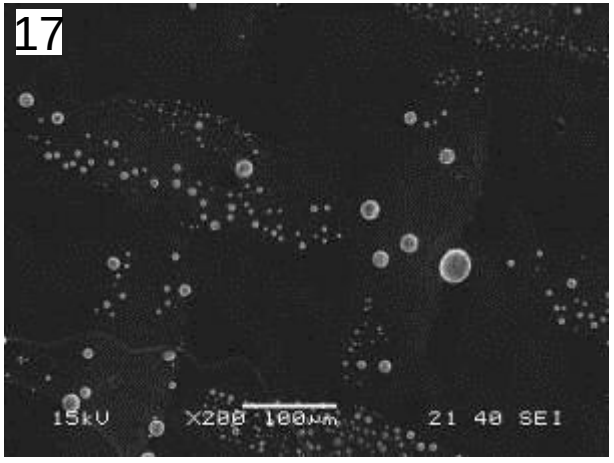




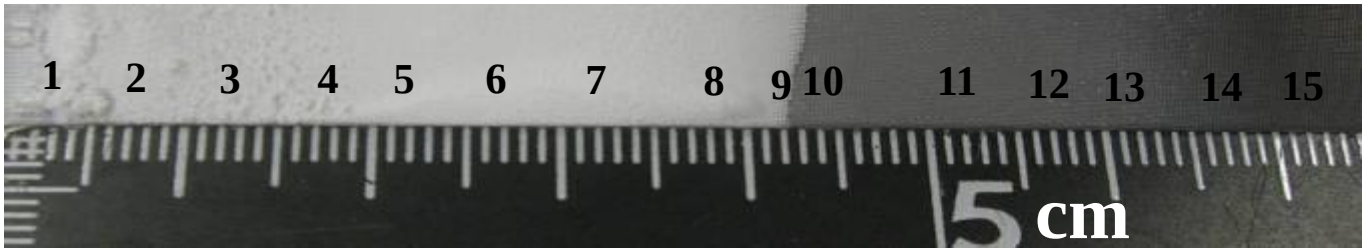




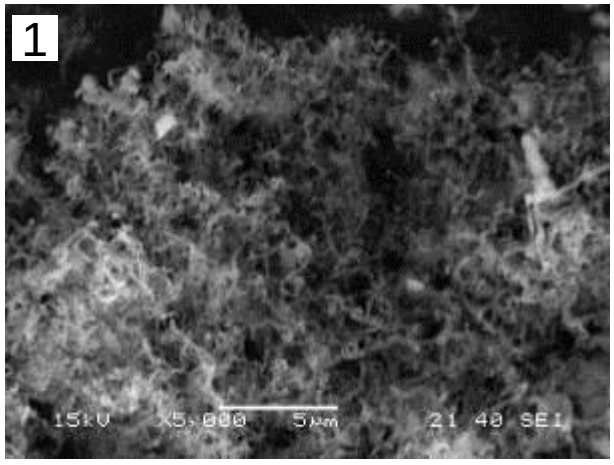


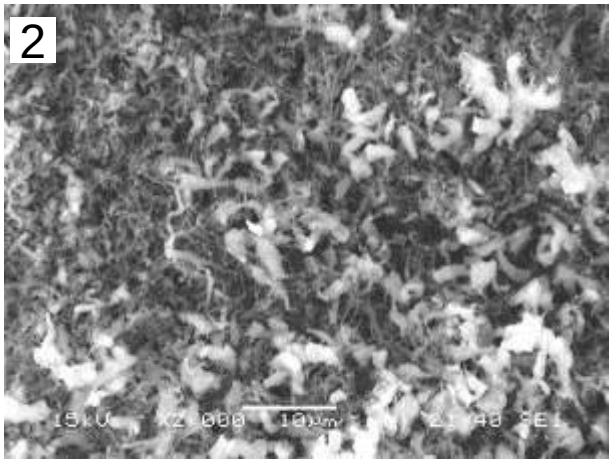


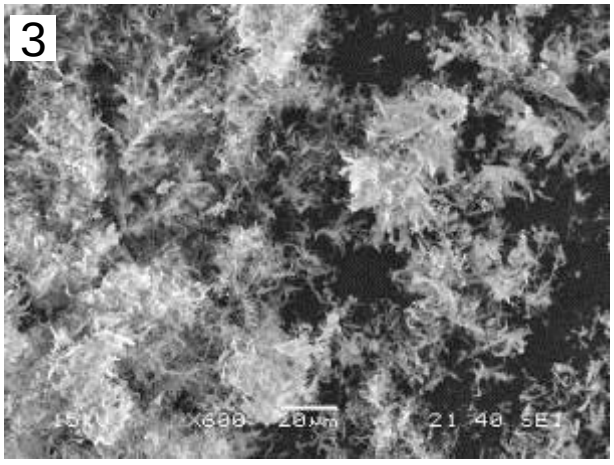
3 MPa-product image

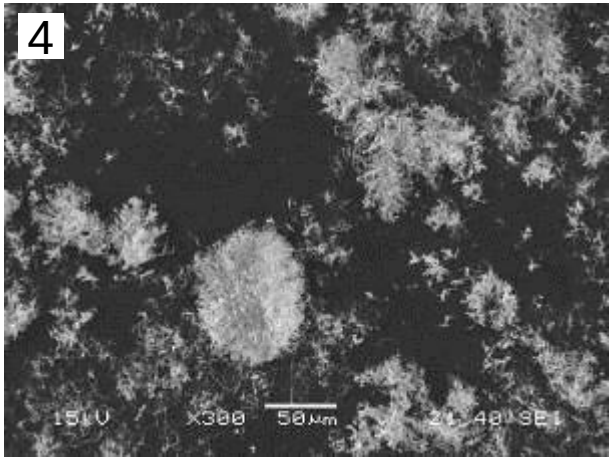


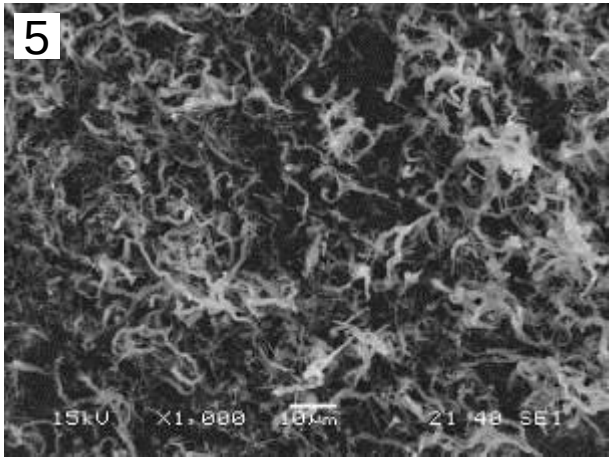
3 MPa-SEM

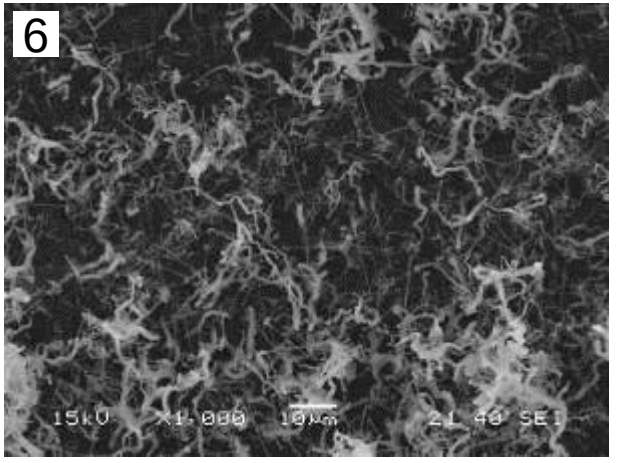

1
15kV X5,000 5μm 21 40 SEI

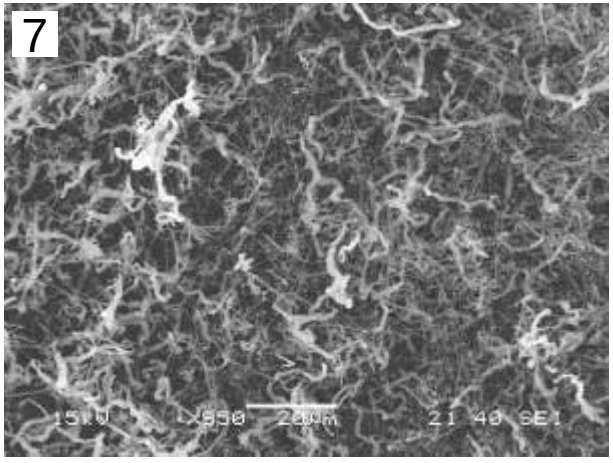

2
15kV X2,000 10μm 21 40 SEI

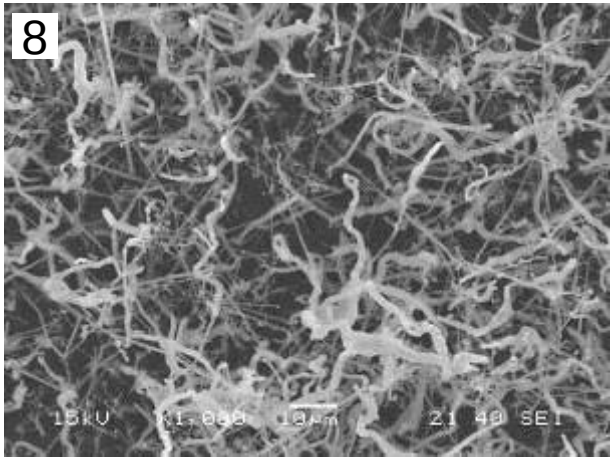

3
15kV X600 20μm 21 40 SEI

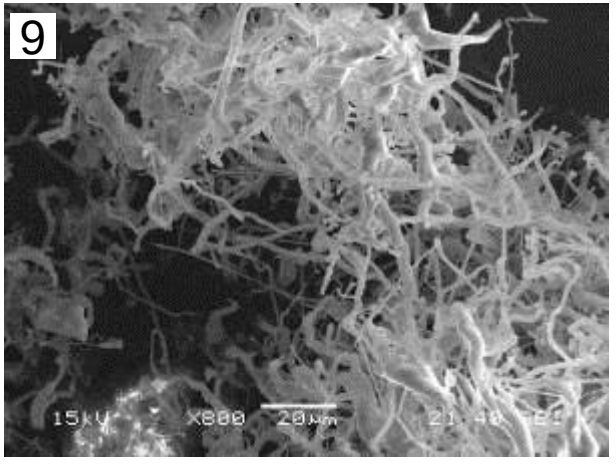

4
15kV X300 50μm 21 40 SEI


5
15kV X1,000 10μm 21 40 SEI

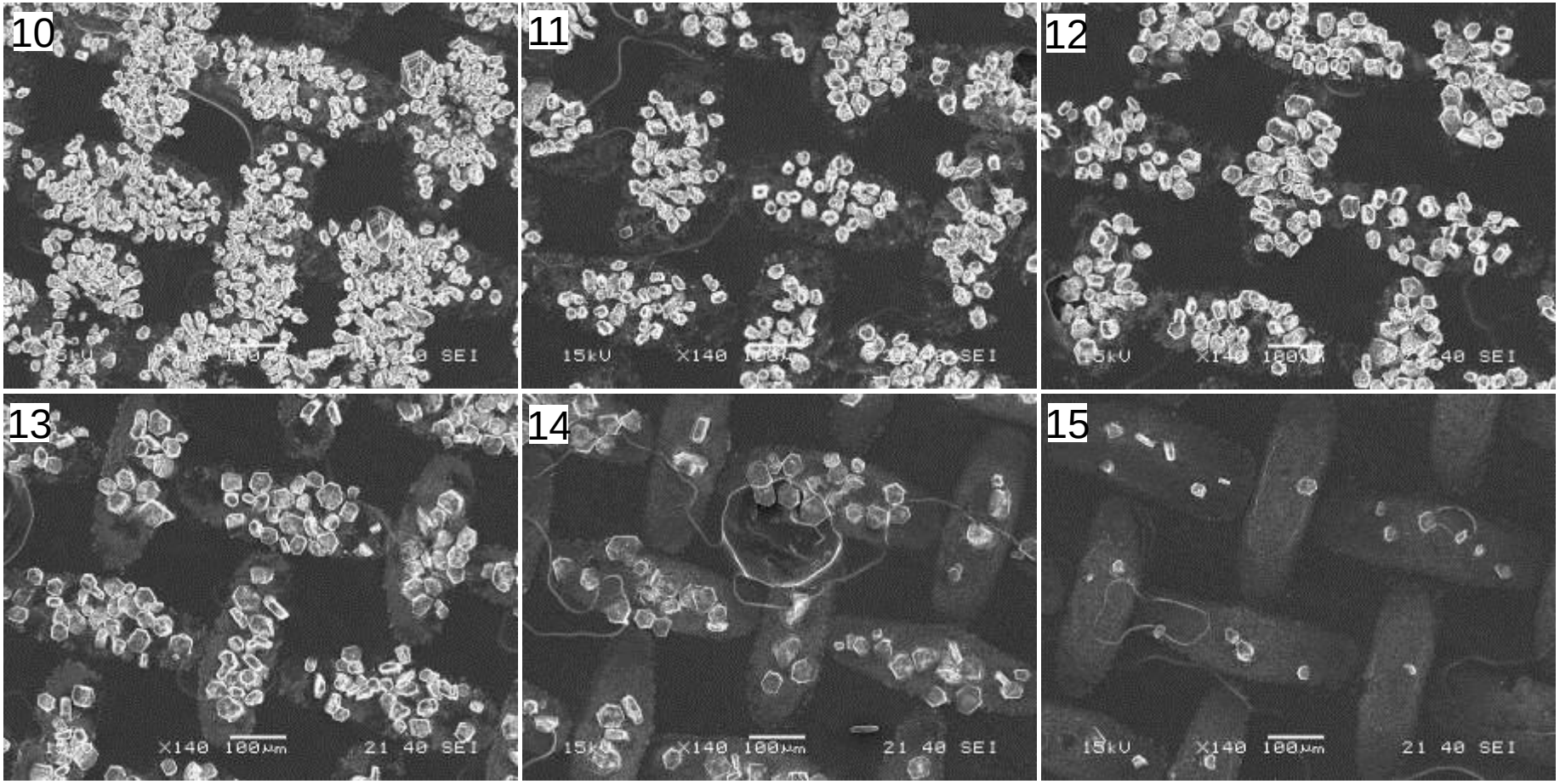

6
15kV X1,000 10μm 21 40 SEI


7
15kV X950 20μm 21 40 SEI

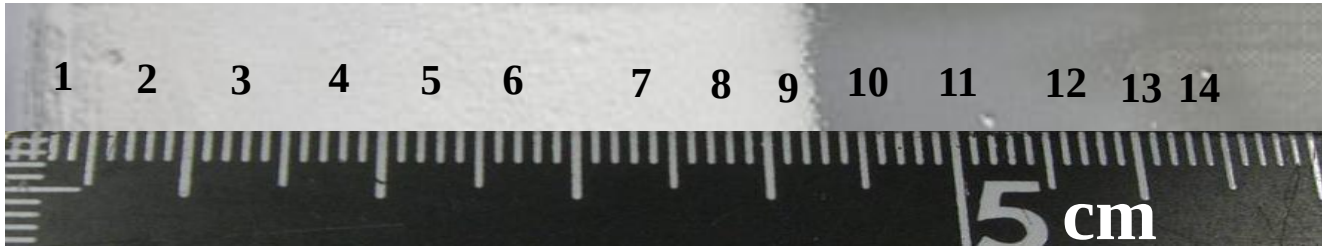

8
15kV X1,000 10μm 21 40 SEI


9
15kV X800 20μm 21 40 SEI

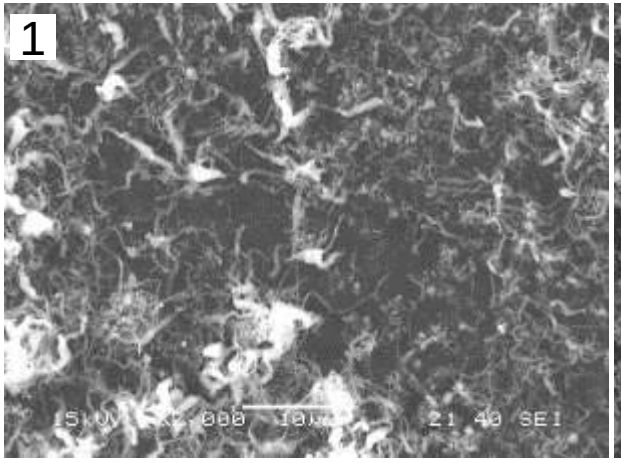
3 MPa-SEM

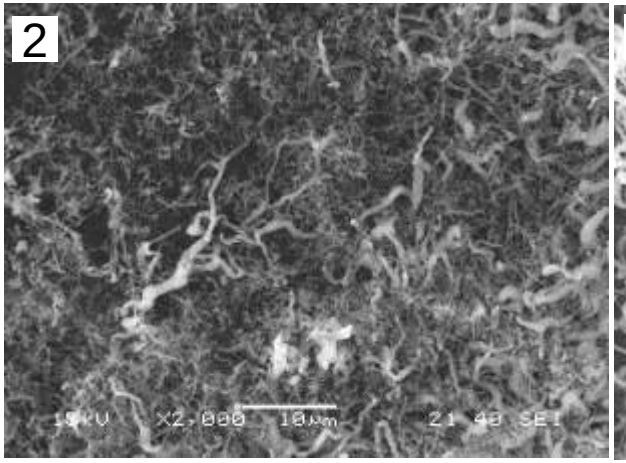


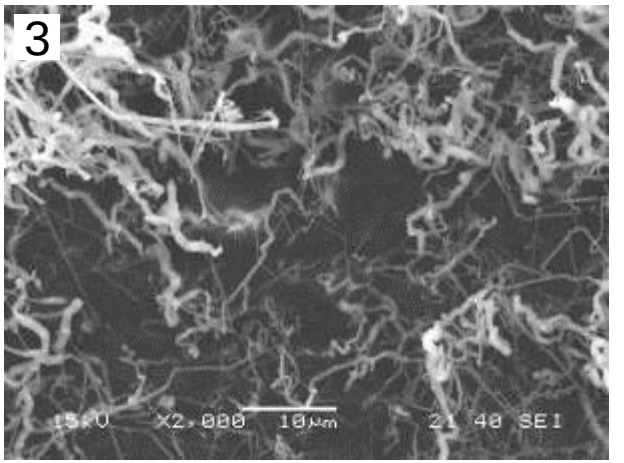
4 MPa-product image

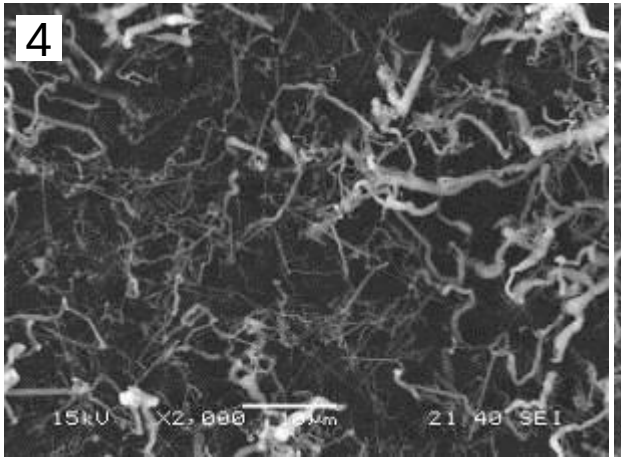


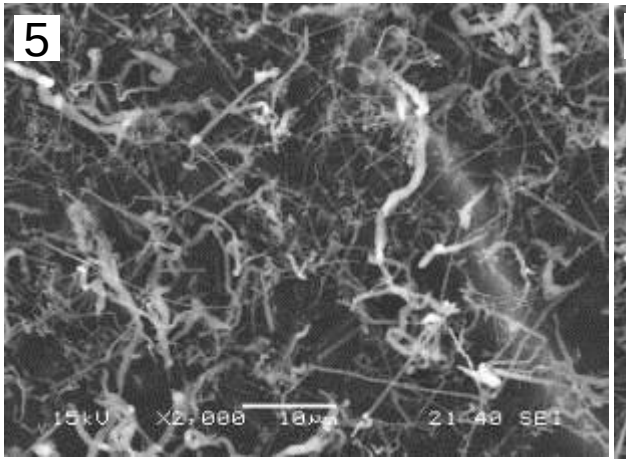
4 MPa-SEM

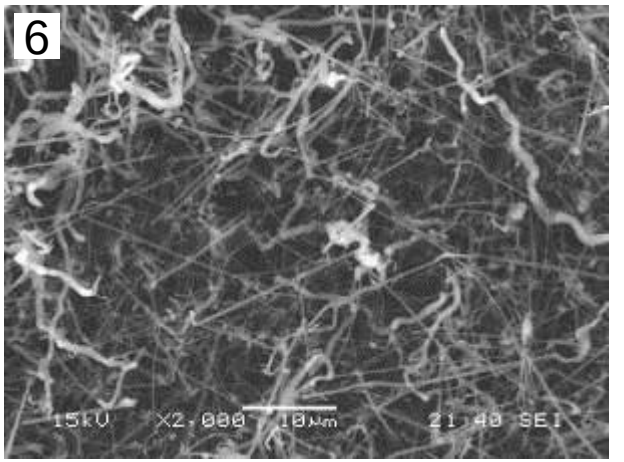

1
15kV X2,000 10μm 21 40 SEI

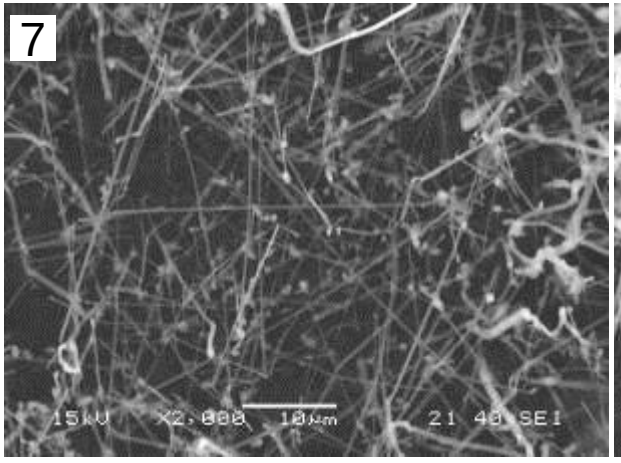

2
15kV X2,000 10μm 21 40 SEI

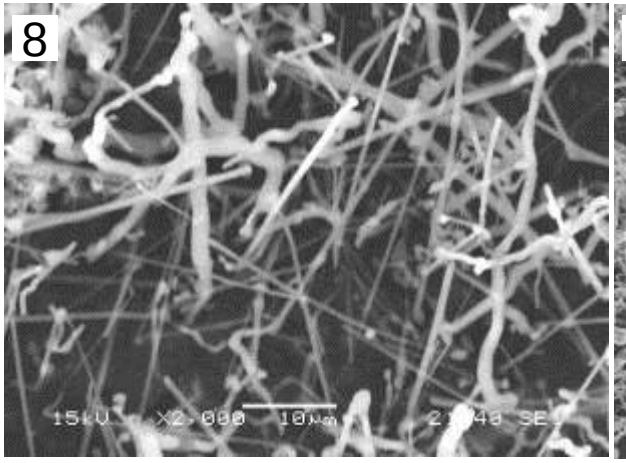

3
15kV X2,000 10μm 21 40 SEI

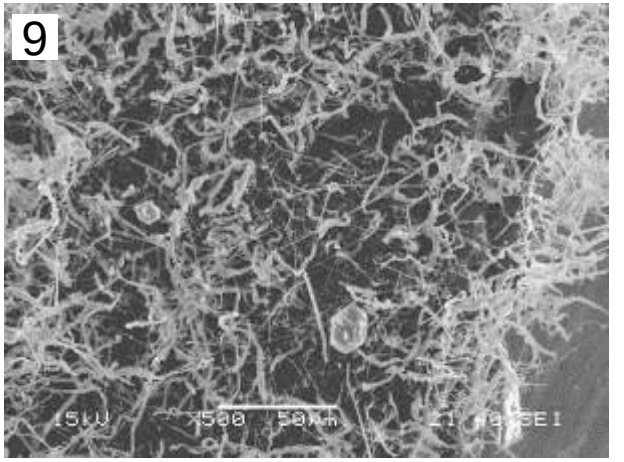

4
15kV X2,000 10μm 21 40 SEI


5
15kV X2,000 10μm 21 40 SEI

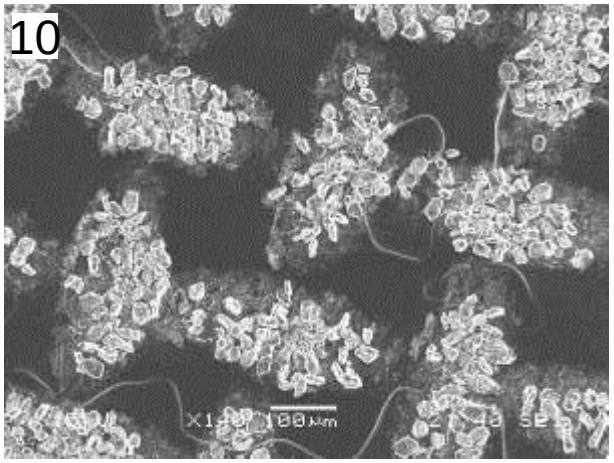

6
15kV X2,000 10μm 21 40 SEI

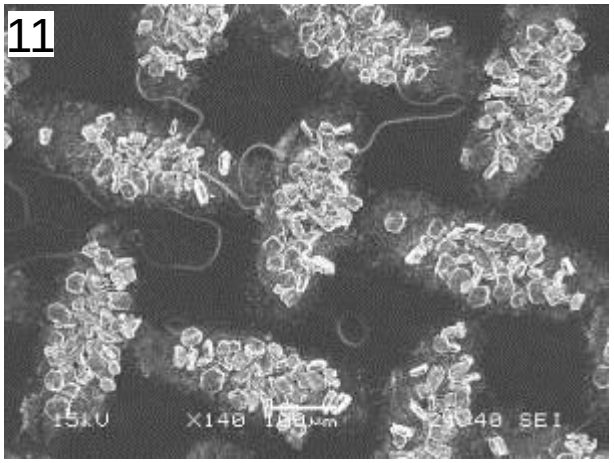

7
15kV X2,000 10μm 21 40 SEI

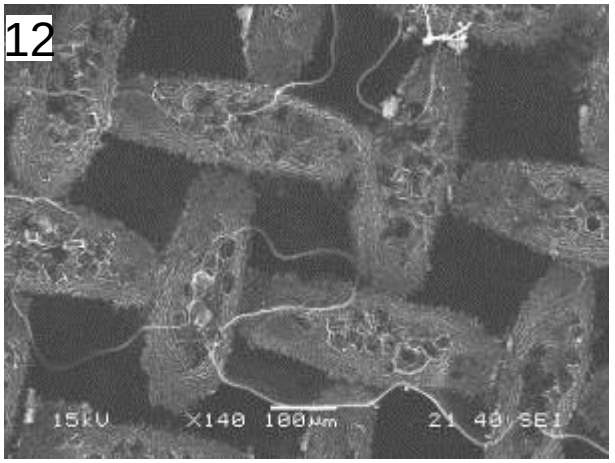

8
15kV X2,000 10μm

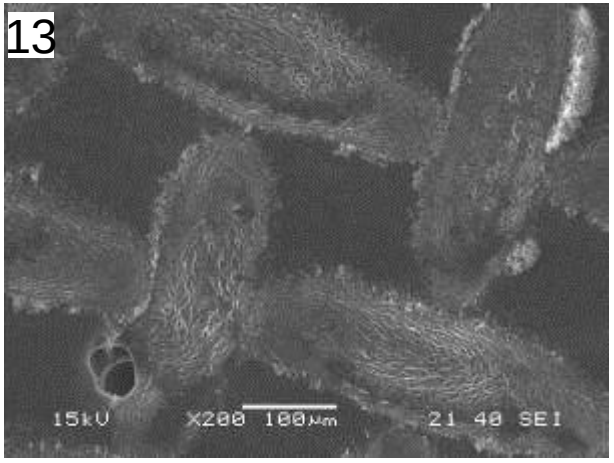

9
15kV X500 50μm

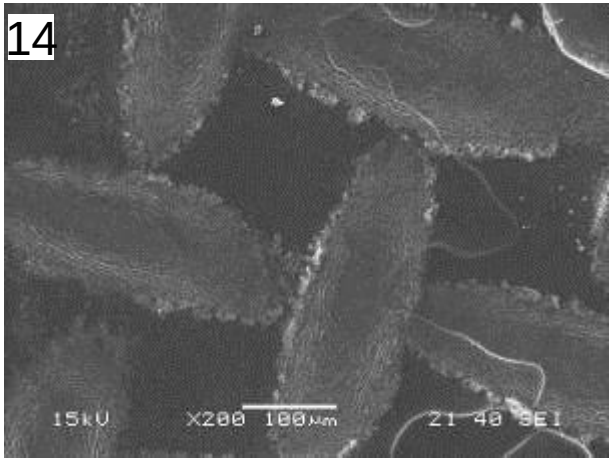
4 MPa-SEM


10


11
15kV X140 100µm 21 40 SEI


12
15kV X140 100µm 21 40 SEI


13
15kV X200 100µm 21 40 SEI


14
15kV X200 100µm 21 40 SEI